The role of latent heating in atmospheric blocking dynamics: a global climatology

Daniel Steinfeld[1] · Stephan Pfahl[1,2]

Abstract

Atmospheric blocking represents an important aspect of the mid-latitude weather variability, but the different processes contributing to its formation and maintenance are not yet fully understood. This study investigates the role that diabatic processes, in particular the release of latent heating in strongly ascending airstreams, play in the dynamics and spatio-temporal variability of blocking in a detailed 38-year global climatological analysis. The results show that the formation and (re-)intensification of blocking are often preceded by latent heating connected to upstream baroclinic developments. While the importance of latent heating varies considerably between individual blocking events and different regions, in particular between ocean and continents, latent heating is generally most important during onset and in more intense and larger blocks. The episodic nature of latent heating during the blocking life cycle, associated with a series of transient cyclones approaching the blocking, can contribute to both the high- (fast onset and fluctuation in intensity and size) and low-frequency (maintenance and quasi-stationarity during maturation phase) properties of blocking anticyclones and provide the required flow amplification in addition to dry-dynamical interaction between synoptic eddies and blocking. This amplification results from a combination of the direct injection of anticyclonic air into the upper-troposphere within cross-isentropic ascending airstreams, setting up large-scale anticyclonic PV anomalies, and the advection of PV by the enhanced divergent outflow at the tropopause (indirect effect). This divergent outflow on the western flank of the blocking anticyclone interacts with the upper-level PV gradient and leads to a westward amplification of the ridge, diminishing the tendency for dissipation and the eastward advection by the background flow, thus contributing to blocking stationarity. Taking into account such diabatic mechanisms in blocking dynamics will be important to improve predictions of blocking and assess future changes in the extratropical large-scale circulation.

Keywords Atmospheric blocking · Atmospheric dynamics · Diabatic processes · Latent heating · Extratropical cyclones · Climatology

1 Introduction

Understanding atmospheric blocking and the underlying physical mechanism responsible for its formation and maintenance has been a key challenge in atmospheric sciences since the first assessments of blocking by Berggren et al. (1949) and Rex (1950). Blocking represents an important aspect of the mid-latitude weather variability, as it describes the formation of persistent, quasi-stationary, large-scale anticyclonic circulation anomalies that disrupt or block the prevailing westerly flow and the eastward progression of synoptic eddies (Rex 1950). Atmospheric blocking occurs when a substantial mass of anomalously anticyclonic potential vorticity (PV) air is advected poleward, related to a meridionally amplified flow, setting up a large-scale anticyclonic PV anomaly in the upper troposphere beneath an elevated tropopause, and a stable surface anticyclone underneath (Hoskins et al. 1985).

Blocking is associated with persistent shifts of the mid-latitude jet stream (Davini et al. 2014; Nakamura and Huang 2018), which then controls the track of cyclonic storm systems (Booth et al. 2017). These persistent changes in the large-scale circulation often lead to anomalous, sometimes

✉ Daniel Steinfeld
dani_steinfeld@hotmail.com

[1] Institute for Atmospheric and Climate Science, ETH Zürich, Zürich, Switzerland

[2] Institute of Meteorology, Freie Universität Berlin, Berlin, Germany

extreme weather such as heatwaves in summer (Pfahl and Wernli 2012) and cold spells in winter (Sillmann et al. 2011; Buehler et al. 2011). Considerable uncertainty of the blocking mechanism still remains and blocking formation is a challenge for numerical weather forecasting (Pelly and Hoskins 2003b; Matsueda 2009), climate models (e.g., Davini and D'Andrea 2016) and future climate projections (e.g., Hassanzadeh et al. 2014; Woollings et al. 2018). Therefore, elucidating the different physical processes that initiate and maintain atmospheric blocking will ultimately improve long-range weather forecasting and projections of the large-scale circulation in a warmer climate.

There is currently no comprehensive theory capturing all aspects of blocking dynamics, and a wide variety of concepts exists (see Tyrlis and Hoskins 2008b; Woollings et al. 2018 for a comprehensive review of blocking theories). Early concepts emphasize the influence of processes occurring on planetary scales, such as wave-resonance (Charney and DeVore 1979) and orography- or thermally-forced stationary waves (Tung and Lindzen 1979; Hoskins and Karoly 1981). However, such processes alone can not explain observed blocking characteristics, such as the rapid onset (with time scales more consistent with synoptic-scale phenomena), the fluctuation in intensity and size and the (eastward) translation during the blocking lifetime (Dole and Gordon 1983; Dole 1986). Particular attention has been given to the dynamical interaction between blocking and synoptic-scale transient eddies, as originally hypothesized by Green (1977) and Shutts (1983), pointing to a central role of extratropical cyclones and anticyclones for blocking formation and maintenance. This perspective highlights the importance of isentropic advection of anticyclonic air masses into the blocking region either by poleward winds ahead of developing baroclinic waves (e.g., Colucci 1985; Mullen 1987; Nakamura and Wallace 1993; Nakamura et al. 1997), the selective absorption of anticyclonic eddies by the block (Yamazaki and Itoh 2012a; Luo et al. 2014), and the role of Rossby wave breaking (Pelly and Hoskins 2003a; Altenhoff et al. 2008; Masato et al. 2012).

All the above listed theories are essentially based on dry dynamics and describe the formation of persistent upper-tropospheric anticyclonic PV anomalies due to isentropic advection of PV. Today, however, moist-diabatic processes, and in particular the latent heating (LH) due to cloud formation in ascending airstreams, are known to play a significant role in modifying the upper-level large-scale flow, including Rossby wave dynamics (e.g., Pomroy and Thorpe 2000; Grams et al. 2011; Wirth et al. 2018). Latent heat release amplifies vertical motion and results in a cross-isentropic ascent and strong divergent outflow near to tropopause. The associated diabatic PV modification leads to a net vertical transport of lower-tropospheric air to higher (isentropic) levels where the background PV is

higher (lower in the Southern Hemisphere) (Hoskins et al. 1985; Wernli and Davies 1997; Methven 2015), deflecting the tropopause poleward and generating anticyclonic PV anomalies in the upper troposphere. In the mid-latitudes, the most intense LH occurs predominantly in the warm conveyor belt (WCB) of extratropical cyclones (Wernli 1997; Madonna et al. 2014), a warm and moist airstream that ascends to the upper troposphere while moving toward polar regions. Also other weather systems, such as large convective systems (Stensrud 2013; Rodwell et al. 2013) or recurving tropical cyclones (e.g., Riemer et al. 2008; Archambault et al. 2013), can exhibit strong diabatic outflow in the vicinity of the jet and modify the tropopause structure in a similar manner.

Given that moist processes can substantially influence Rossby wave dynamics, this suggests that LH may also modify the development of atmospheric blocking that is intimately linked to the development of Rossby waves. Some case studies have pointed to such effects of LH on blocking (Schwierz 2001; Tilly et al. 2008; Croci-Maspoli and Davies 2009; Parker et al. 2013; Cheung et al. 2013), however, only recently Pfahl et al. (2015) quantified this contribution of LH for blocking, revealing that moist-diabatic processes and the cross-isentropic transport of mass are of similar importance for blocking formation and maintenance as dry-adiabatic processes (isentropic mass transport).

Nevertheless, the effect of moist processes and associated latent heat release on blocking dynamics and variability remains not well understood, mainly because it influences the large-scale flow in a complex nonlinear way and is tightly coupled to the dry dynamics of baroclinic waves (e.g., Kuo et al. 1990; Teubler and Riemer 2016). In addition, there are large uncertainties in where, when and how LH influences the onset, maintenance and decay of blocking that is otherwise determined by dry dynamics. Furthermore, the importance of LH can be expected to vary in a warmer future climate due to increased atmospheric moisture content (Schneider et al. 2010) and changes in mid-latitude jetstream variability (Barnes and Screen 2015). A key step toward better understanding and predicting atmospheric blocking is to characterize how LH affects the life cycle of blocking. In this study, we will use a combined Lagrangian-Eulerian approach to examine the role of LH in ascending airstreams for blocking dynamics from a detailed climatological perspective using reanalysis data as described in Sect. 2. We will build on the results of Pfahl et al. (2015), but go substantially beyond this study by (i) presenting a global climatology of blocking in Sect. 3, (ii) fully characterizing the case-to-case and spatio-temporal variability of LH and identifying environmental conditions and forcing mechanism for ascent and LH (Sect. 4) and (iii) analyzing the dynamical link between LH, upstream cyclones and the structure and life cycle of blocks in Sect. 5. Our results are summarized,

discussed and put into perspective with the more traditional blocking concepts in Sect. 6.

2 Data and methods

2.1 Data

This study is based on global 6-hourly ERA-Interim reanalysis data (Dee et al. 2011) on a $1° \times 1°$ regular grid with 60 vertical levels for the period 1979–2016. Climatological means and anomalies in this study always refer to calendar-month averages over the 38-year period. Note that the term "upper-level" will be used hereafter to describe the vertically averaged flow between 500 and 150 hPa. The term "anticyclonic PV" will be used for anomalously low-PV air in the Northern Hemisphere and anomalously high-PV air in the Southern Hemisphere.

2.2 Blocking identification and tracking

Atmospheric blocking covers a variety of flow patterns, including amplified stationary ridges, Ω-shaped blocks or high-over-low dipole blocks (see Fig. 1 in Woollings et al. 2018). Hence, different approaches to identify blocks have been developed (see Barnes et al. 2012; Barriopedro et al. 2010, for in-depth summaries of blocking detection methods). In order to have a representative sample of blocking flow patterns and to estimate the sensitivity of the results to the choice of identification method, we employ two different methods: a PV-anomaly-based (APV) and an absolute geopotential height reversal-based (AGP) blocking index.

Following Schwierz et al. (2004), the APV index identifies and tracks individual blocks (the term "block" and "blocking event" are used as synonyms here) from genesis to lysis as upper-level anticyclonic PV anomalies that exceed -1.3 potential vorticity units [pvu; 1 pvu $= 10^{-6}$ K kg^{-1} m^2 s^{-1}; note that PV values are multiplied by -1 in the Southern Hemisphere], spatial overlap by 70% between successive 6-hourly time steps and persist for at least 5 consecutive days. The advantage of the APV index is that it objectively captures the core of the anomalous anticyclonic circulation and thus directly allows for an investigation of the origin and evolution of individual blocks and the associated air masses. In addition, by allowing for moderate displacements of the anticyclonic anomalies (70% spatial overlap), blocks are identified in an earlier stage of their life cycle during rapid ridge amplification of transient Rossby waves into a large-amplitude block. The APV blocking climatology used here is publicly available via an ETH Zurich-based web server [http://eraiclim.ethz.ch/, see Sprenger et al. (2017)].

We additionally use the AGP approach by Scherrer et al. (2006) to identify blocked regions in a latitude band between 45 and 75° N/S, with a spatial overlap for at least 5 days, based on a reversal of the geopotential height gradient at 500 hPa (Z500). Lower latitudes are excluded here to avoid the identification of subtropical highs, which are different dynamical features. The index is a two-dimensional extension of the classical blocking index by Tibaldi and Molteni (1990), which follows the original description of Rex (1950). The AGP index captures mature blocking phases with wave breaking characteristics and identifies the flanks of the anticyclonic circulation anomalies where the westerly winds are reversed. Here this index is used to test the robustness of the main climatological results with respect to the choice of the blocking index. When not explicitly stated otherwise, the results are only presented for the APV index.

2.3 Trajectory calculation and latent heating

To quantify the relative contribution of dry and moist processes to blocking, we compute kinematic 7-day backward air-parcel trajectories based on the three-dimensional winds using the Lagrangian Analysis tool LAGRANTO (Wernli and Davies 1997; Sprenger and Wernli 2015). The trajectories are started from an equidistant grid ($\Delta x = 200$ km horizontally and $\Delta p = 75$ hPa vertically between 500 and 125 hPa) located in a blocking region at each six-hourly time step, with the additional criterion that PV must be smaller than 1 pvu (larger than -1 pvu in the SH) to exclude points located in the stratosphere. Various variables such as PV, potential temperature θ and specific humidity are traced along the blocking trajectories, and the Lagrangian changes of these variables are evaluated statistically. Since both PV and θ are conserved for adiabatic and frictionless motion, changes in these variables between two time steps along a trajectory are attributed to diabatic processes, such as cloud formation, radiation and friction. This Lagrangian investigation of blocking air masses captures the full three-dimensional complexity of diabatic processes. An important limitation of this approach is that trajectories follow the resolved large-scale wind and do not capture fast convective motions. This might introduce an underestimation of the relevance of LH.

In addition to the direct diabatic PV modification, there are also other indirect effects by which LH can influence the upper-level flow, namely LH amplifies vertical motion and results in an enhanced divergent outflow near the tropopause (e.g., Riemer and Jones 2010). Therefore, we also compute the upper-level PV advection by the divergent and non-divergent wind components. A detailed description of the calculation can be found in Sect. 5.

A total of 4270 atmospheric blocking events are identified globally from 1979 to 2016 with the APV index, and around 28.6 million blocking trajectories have been calculated. The number of blocking events in the NH (2558) is 1.5 times

higher than in the SH (1712). For AGP blocks, which are less frequent, 5.1 million trajectories have been calculated.
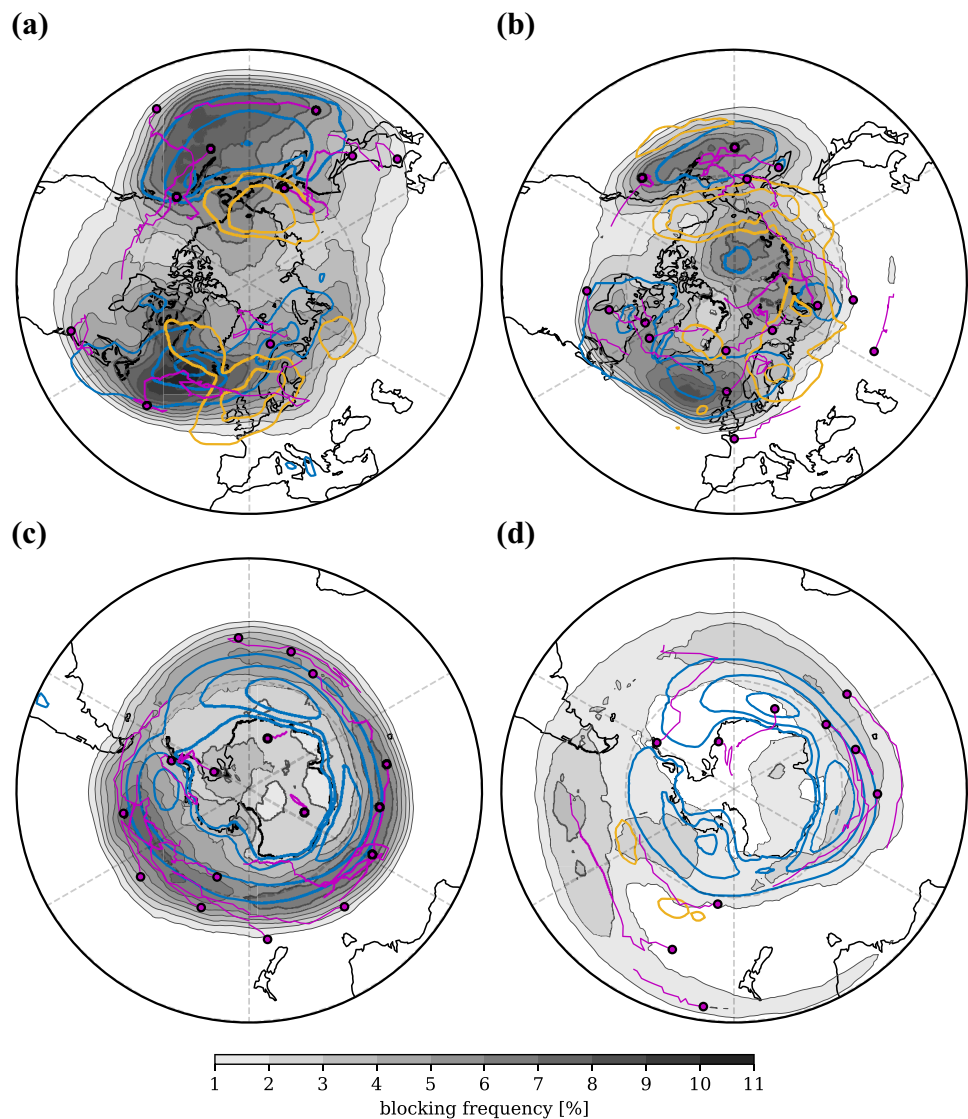
3 Blocking climatology

For reference, it is pertinent to start the analysis with a discussion on the blocking climatology. The seasonal frequency distributions of atmospheric blocking are shown in Fig. 1. In addition, as an example tracks and genesis positions of blocking anticyclones for the year 2015 are indicated by the solid magenta lines and filled circles, respectively.

In agreement with previous studies for the Northern Hemisphere (NH) (e.g., Dole and Gordon 1983; Lejenäs and økland 1983), blocking occurs most frequently over the North Atlantic/Europe and the North Pacific. Blocking frequencies are highest (more than 10%) in winter (DJF), as

well as in autumn (SON) and spring (MAM) (not shown), and generally decrease in summer. The low frequencies in summer are related to the fact that anticyclonic PV anomalies are generally weaker. Secondary weaker maxima occur over the Asian continent downstream of the Ural Mountains, most evident during the equinoctial seasons (not shown), and at high latitudes in summer. For a more detailed description of the seasonal and regional blocking variability, the reader is referred to the comprehensive climatology presented by Croci-Maspoli et al. (2007) using ERA-40 data, which closely agrees with our climatology.

In the Southern Hemisphere (SH), the blocking frequency is weaker and much more zonally symmetric than in the NH and found over the Southern Ocean around the entire hemisphere. The high frequencies in the east Pacific sector and the reduced frequencies in the whole SH during local winter (JJA) resemble the results of previous studies (e.g.,

Fig. 1 Spatial distributions of blocking frequency based on the APV index for the NH (top panels) and the SH (lower panels) during DJF (left) und JJA (right) 1979–2016 (gray shading). Units are percentage of blocked days relative to the total number of days per season. In addition, genesis points and tracks (location of the center of mass) for blocks in 2015 are shown in magenta. Cyclone frequency is shown with blue contours (20, 30, 40, 50%), and the AGP blocking frequency as yellow contours (2, 4%, smoothed with a 2° averaging radius)

Renwick 2005; Berrisford et al. 2007). Blocking activity is also found at very high latitudes.

While our blocking climatology agrees well with other anomaly-based indices (e.g., Dole and Gordon 1983; Small et al. 2013), indices based on the reversal of the climatological westerly flow, measured in terms of the gradient of the mid-tropospheric geopotential height (AGP, Scherrer et al. 2006) or potential temperature on the dynamical tropopause (Pelly and Hoskins 2003a), typically yield a shift in location. Europe, Greenland and the high-latitude North Pacific are the most distinctive areas of AGP blocking activity (yellow contours in Fig. 1). This shift is a consequence of the APV blocks being identified earlier in their life cycle, during rapid amplification of transient Rossby waves which constitute precursors of blocking, whereas reversal indices mainly capture the flank of mature blocking anticyclones with wave-breaking characteristics (e.g., Scherrer et al. 2006; Barriopedro et al. 2010). In addition, over the North Pacific ocean and in the SH AGP blocks are also less frequent, probably because in these regions so-called Ω blocks are more common (Sumner 1955), which do not exhibit the same strong easterly flow as Euro-Atlantic dipole blocks (Altenhoff et al. 2008). Despite these differences, the two indices (AGP and APV) typically identify comparable dynamical anomalies of the mid-latitude flow, as validated in case studies (see also Scherrer et al. 2006; Pfahl et al. 2015).

The exemplary blocking tracks for the year 2015 shown in Fig. 1 provide information about typical blocking pathways, genesis and lysis regions. Tracks are only shown for one year for clarity, but these tracks are representative for the entire climatology. In general, blocking anticyclones move eastward with a more poleward (equatorward) component during their early (later) stages. In the SH, tracks typically are zonally oriented. The tracks show that most blocking events over Europe and North America originate upstream over the ocean. Although the mean propagation of blocks is towards the east (Croci-Maspoli et al. 2007; Ioannidou and Yau 2008), a clear signal of retrogressing of individual blocks can be observed (see also Lejenäs 1984).

Figure 2 shows the distributions of the mean zonal propagation velocity of the center of mass of APV blocks during the entire lifetime, as well as only during onset (days 0–2) and mature (days 3–5) phases. Note that this is only a rough estimate, since the center of mass can sometimes move around without major shifts of the entire blocking system. The vast majority of APV blocks are slowly moving systems with a mean zonal speed of median 3.5 m s^{-1}. This is considerably slower than the typical phase speed of transient upper-level waves of about 12 m s^{-1} (e.g., Chang and Yu 1999, for NH winter). It is noteworthy that the mean zonal propagation speed of APV blocks decreases during mature phase (yellow distribution with median of 2.9 m s^{-1}), which is the time when AGP blocks are likely
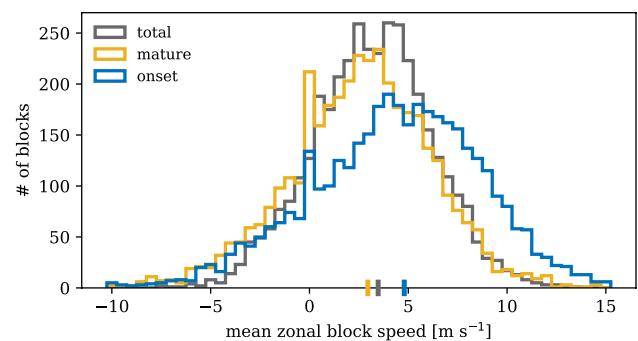
Fig. 2 Distributions of mean zonal propagation speed during the entire lifetime (gray), onset (days 0–2, blue) and mature (days 3–5, yellow) phases for all 4270 APV blocks. The median for each distribution is shown on the horizontal axis

to occur, compared to the onset (blue distribution with median of ~ 5 m s^{-1}), which is characterized by fast ridge amplification of transient synoptic-scale waves (Altenhoff et al. 2008). It should be noted that the APV blocking algorithm detects a small fraction of rapidly traveling anticyclones (2% with > 10 m s^{-1} during mature phase), which may not be considered as classical blocks. Blocks have an average lifetime, plus/minus one standard deviation, of 8.4 ± 4 days. 23.2% of all blocks are long-lived systems with a lifetime ≥ 10 days, the maximum is 48 days. The seasonal and regional variability in blocking duration is generally small. On average, oceanic winter blocks have the longest (~ 10 days) and continental winter blocks have the shortest (~ 8 days) lifetime. NH blocks have a mean lifetime of ~ 9 ± 4.4 days, which is slightly longer than their SH counterparts (~ 8 ± 3.2 days). Shorter SH blocking duration is attributed to the generally stronger westerlies in the SH (Trenberth and Mo 1985; Lupo and Smith 1995; Wiedenmann et al. 2002).

Because rapidly moving cyclones (transient eddies) and blocking are linked by strong dynamical interactions (see Sect. 1), we discuss briefly the spatial relationship between the main blocking and climatological storm track regions. To characterize the storm tracks, extratropical cyclone frequencies are calculated using a slightly updated version (Sprenger et al. 2017) of the algorithm of Wernli and Schwierz (2006). The major blocking areas are situated in the proximity of the main storm tracks (blue contours in Fig. 1), and both feature similar spatial patterns and seasonal progression, e.g. the northward tilt over the North Atlantic in DJF and the equatorward shift in the South Pacific during the presence of a split jet in JJA. Blocking frequency maxima are shifted slightly equatorward compared to the storm tracks, particularly in the SH. This spatial offset is likely related to the fact that cyclones are typically located on the poleward side of the jet during the end of their life cycle (Oruba et al. 2013), while mid-latitude blocking, often characterized by

anticyclonic wave breaking, is located on the equatorward side (Masato et al. 2012). AGP blocks are found on the eastern (over Europe) and poleward (over North Pacific) flank of the storm tracks (see also Zappa et al. 2014). This geographical co-occurrence points to a strong dynamical interactions between blocking and extratropical cyclones, as will be further discussed below.

4 The role of latent heating

4.1 Climatology of blocking air masses

In this section, we quantify the fraction of blocking air masses that are diabatically heated during the three (or seven) days prior to reaching the blocking region. To this end, we calculate the maximum latent heating ($\Delta\theta$), which is defined as the difference between the maximum value of θ and the preceding minimum value during a specific time period (seven or three days) along the backward trajectories. Following the approach of Pfahl et al. (2015), a threshold of $\Delta\theta > 2$ K is used to identify blocking air masses that have experienced distinct latent heat release. In addition, the maximum latent cooling is calculated for blocking air masses if the following two conditions are met: $\Delta\theta < 2$ K and the maximum cooling is larger than the maximum heating. In the following climatological analysis, for each trajectory either only the heating or only the cooling is considered to avoid cancellation effects of heating and cooling along the flow. The importance of LH is quantified by the percentage of diabatically heated trajectories ($\Delta\theta > 2$ K) compared to all trajectories that are attributed to a blocking (in the following denoted LH contribution). The LH contribution is also an effective measure of the strength of latent heat release in K along the trajectories, as it is correlated to the mean changes in θ along the trajectories with a Spearman rank correlation coefficient of 0.9.

Figure 3 shows the statistical distribution of $\Delta\theta$ during the three-day (solid lines) and seven-day (dashed lines) periods for blocking defined with the APV-based (yellow lines, ~ 28.6 million trajectories) and AGP-based (gray lines, ~ 5.1 million trajectories) indices. The distributions reveal that the flow is actually never perfectly adiabatic. Two regimes can be identified in this figure: a no-heating "cooling" regime [called quasi-adiabatic regime in Pfahl et al. (2015)], and a heating regime with a wide range of $\Delta\theta$ up to 30 K. A threshold of $\Delta\theta = 2$ K is used to separate these regimes and to select blocking air masses affected by distinct LH. Considering a time period of three days (solid lines), 46% (31.1% for AGP) of the blocking air masses experience heating of more than 2 K. These high fractions demonstrate the overall relevance of diabatically produced anticyclonic PV anomalies for atmospheric blocking (see again Pfahl et al.
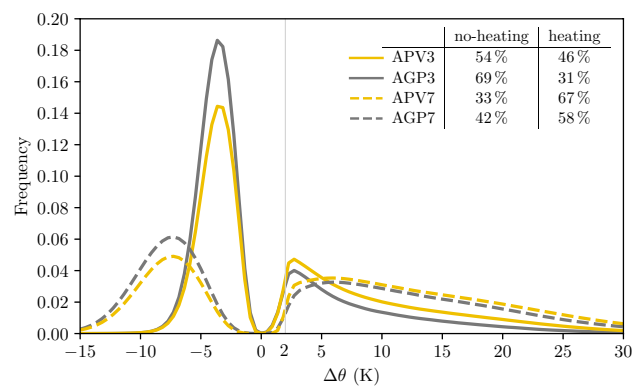
Fig. 3 Frequency distributions (probability density) of maximum potential temperature change along backward trajectories during three days (solid lines) and seven days (dashed lines) before their arrival in the blocking region for APV (yellow lines) and AGP (gray lines) blocks. Percentages of blocking air parcels in the two regimes defined by $\Delta\theta = 2$ K are given

2015). The trajectories of the heating regime exhibit strong heating of 8.5 K in the median, and the concurrent loss of specific humidity of 2.5 g kg^{-1} and ascent of around 300 hPa (not shown) indicate that cloud formation plays the dominant role for this pronounced cross-isentropic flow of air into the blocking anticyclones. These trajectories typically reach higher altitudes within the blocking region compared to trajectories in the no-heating regime (see Fig. S7 in Pfahl et al. 2015), which is important since PV anomalies are only generated when air with tropospheric PV can reach regions with stratospheric PV values. If $\Delta\theta$ is evaluated along an extended period of seven days (dashed lines in Fig. 3), latent heating is even more important. On this timescale, 67.4% (58.4% for AGP) of the blocking air masses experience LH of $\Delta\theta > 2$ K with a median heating of 12.3 K.

The no-heating regime ($\Delta\theta < 2$ K) comprises 54% (68.9% for AGP) of the blocking air masses. Most trajectories in the no-heating regime experience diabatic cooling of median -3.7 K before arriving in the blocking region, most probably caused by long-wave radiative cooling (Ferreira et al. 2016), which is in agreement with the trajectories' weak descent in the upper troposphere (not shown). They remain exposed to radiative cooling at a fairly constant rate of about 1 K day^{-1}, which is the expected value experienced by near-tropopause air masses (Hoskins et al. 1985). Interestingly, 21% of the air masses in the no-heating regime (and 9.5% of all blocking trajectories) are already located in the blocking region at day -3 and are thus upper-level air masses that recirculate within the blocking anticyclones. Although the trajectories in the no-heating regime are cooled between day -3 and day 0, a large fraction (50%) is actually heated diabatically (median heating of 11.9 K) between day -7 and day -3 in remote regions and then advected with the upper-level westerlies into the blocking anticyclones during the final 3 days, which

explains the substantial increase in the number of heated trajectories for a time period of seven days.

9.7% (4.3%) of all bocking trajectories are identified as warm conveyor belts (WCB) that ascend more than 600 hPa within 48 h (Madonna et al. 2014) during 7 (3) days before reaching the blocking region, and thus experience even stronger LH of Δθ= 25.1 K in the median. However, the distribution in Fig. 3 shows that the main contribution to blocking comes from shallower ascents.

When using the AGP index to identify blocking, the number of heated trajectories is lower on a three-day timescale, but more comparable to the APV index for a seven-day timescale, which can be explained by the typical temporal and spatial configuration: AGP blocks are detected later in the blocking life cycle compared to APV blocks and are mostly located near the exit region of the storm tracks (see Fig. 1), and thus further downstream from the region where, climatologically, latent heat release is largest (see Sect. 4.3).

In summary, this analysis highlights the contributions of both moist-diabatic processes (cross-isentropic mass transport) and quasi-adiabatic (weak cooling) processes (quasi-isentropic mass transport) for upper-level anticyclonic PV anomalies that characterize blocking. In the following sections, we focus on the role of LH in ascending airstreams for the seasonal and spatial variation as well as the life cycle of blocking events. A detailed investigation of the origins of quasi-isentropic blocking trajectories has been provided by Yamazaki and Itoh (2012a, b) and Pfahl et al. (2015). The role of diabatic cooling in the upper troposphere, which typically weakens the anticyclonic PV near the tropopause (by ∼ 0.02 pvu in 3 days along no-heating trajectories, not shown), is not investigated here.

4.2 Case-to-case and spatio-temporal variability

Despite the relatively large contribution of diabatically heated air masses to blocking, the question remains if temporal and spatial variability of blocking occurrence can be linked to cloud-diabatic activity. Hence, we now examine the seasonal, regional and case-to-case variability of the importance of LH for blocking.

Figure 4 shows the averaged LH contribution (% trajectories heated by more than 2 K averaged over the entire blocking life span) for all 4270 blocking events for the NH and SH. The distributions reveal that the case-to-case variability in the strength of the LH contribution between blocking events is substantial and that moist-diabatic processes are thus not equally important for all blocks. While for most blocks between 35 and 55% (with a median value of 45%) of their air masses have been heated diabatically during the last 3 days, some blocks have a very small LH contribution (minimum is 0%, meaning that no blocking air mass was diabatically heated by more than 2 K during the last 3 days, which is the case for 5 high-latitude blocks), and others have a larger LH contribution, sometimes even exceeding 70% (maximum is 87%). If LH is evaluated along an

Fig. 4 Contribution of diabatically heated trajectories [%] for individual blocking events in **a** Northern Hemisphere (n = 2558) and **b** Southern Hemisphere (n = 1712) evaluated along 3 and 7 day backward trajectories. The boxes show 25, 50, 75% percentiles, the whiskers the 5 and 95% percentiles. Markers show medians for DJF (blue) and JJA (yellow) for different regions
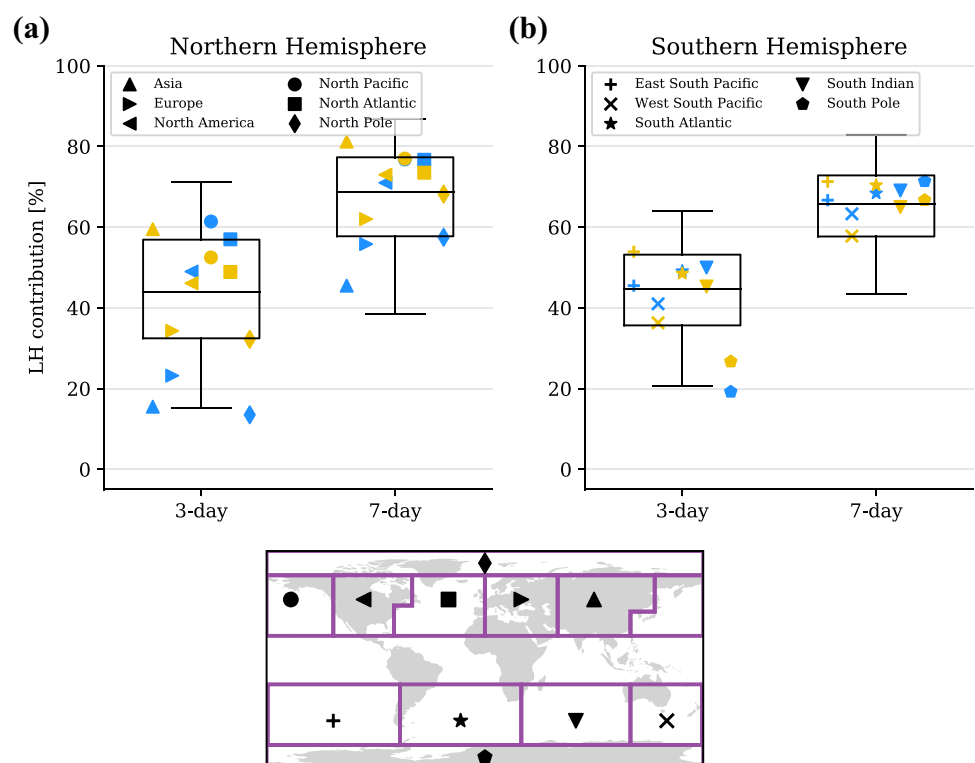
extended time period of seven days along the trajectories (right boxplots in Fig. 4), diabatic heating is more important for almost all blocks with a median value of 67%. This large case-to-case variability in the LH contribution shows that different (dry- or moist-) dynamical processes can dominate for individual blocking events.

The importance of LH does not vary substantially between the NH and SH. The NH distributions show a slightly larger case-to-case variability. Seasonal variations (averaged over a hemisphere) are on the order of a few % (not shown). However, regional differences (ocean vs continent) can be substantial, as discussed in the following.

The global distribution of the mean LH contribution for DJF and JJA is shown in Fig. 5a, b. In addition, markers in Fig. 4 show the median LH contribution for different regions. There are distinct regions where diabatic heating is particularly important (yellow to reddish shading in Fig. 5a, b). In general, the lowest LH contributions, and thus regions where dry dynamics (quasi-adiabatic mass transport) dominate, are typically found at very high (polar) latitudes. In the NH, there are pronounced changes between the seasons (largest differences are between DJF and JJA) and a strong land - sea contrast. Blocks over the oceans typically exhibit high LH contribution throughout the year (average values > 50%), while continental blocks exhibit strong seasonality, which is most pronounced over the Asian continent (see upright triangle in Fig. 4a), with low values in winter and high values in summer. During DJF, the LH contribution peaks over the western part of the North Atlantic and over

the entire North Pacific extending eastward to North America, and reduces to a minimum (< 30%) over the Eurasian continent. The spatial patterns shift in JJA, when maximum LH contribution are also found over land, particularly over northern Asia and eastern North America, and still over the North Pacific. Regions of low LH contributions in JJA are Europe and western North America. Blocks located over Europe typically experience low to moderate LH contribution throughout the year, but the values increase drastically when considering LH along 7-day blocking trajectories (around 60%, Fig. 4a). Likewise, for Arctic blocks the LH contribution is low when considering a 3-day period and strongly increase for a 7-day period. This indicates that air masses that quasi-adiabatically enter these blocks experienced diabatic heating more than 3 days before and further upstream over the subtropical or mid-latitude oceans, and are then advected with the upper-level westerlies into the blocking region.

In the SH, the zonal and seasonal variations are less pronounced, with the greatest LH contributions over the eastern South Pacific, South Atlantic and South Indian Ocean, and regions of low LH contribution in the Australia-New Zealand region, southeast of South America and at very high latitudes. Again, LH contributions increase substantially when considering diabatic heating along 7-day period (Fig. 4b), pointing to the importance of LH over remote regions.

Figure 5c,d show the mean change in θ along all trajectories at the respective blocking location, highlighting regions where blocking air masses are generally affected by stronger

Fig. 5 Spatial distribution of **a**, **b** the mean LH contribution (%, calculated as the mean percentage of trajectories with Δθ > 2 K) and **c**, **d** mean Δθ (K, calculated as the mean change in θ along all blocking trajectories) for all blocking events at the respective location along their track during DJF (left) and JJA (right). Only regions where the blocking frequency exceeds 1% are displayed. White contours show blocking intensification frequency (2 and 4%, relative to the total number of days per season, smoothed with a 2° averaging radius). Black (gray) crosses show the locations of blocking centers during strongest intensification for the 5% blocks with strongest (weakest) LH contribution
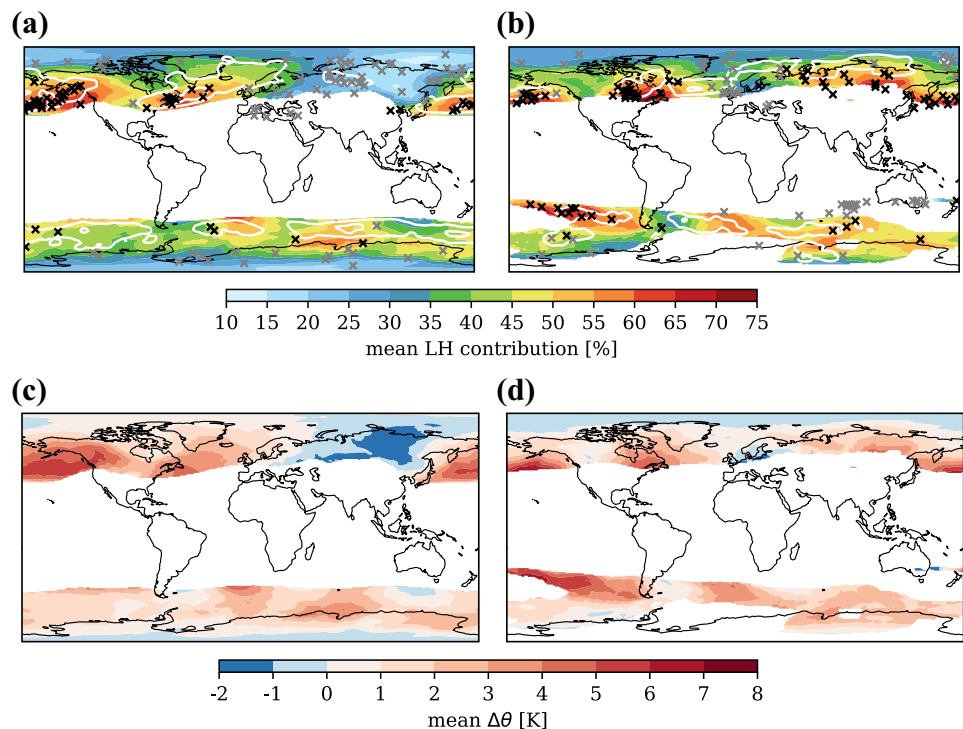
or weaker heating. It shows a similar spatial and seasonal pattern as the mean LH contribution. Over the oceans, where the LH contribution is high, mean heating can be very strong (up to 8 K), but also in other regions, where the LH contribution is below 45% and thus the majority of the trajectories are cooled, the net effect of all trajectories is a heating. This is due to the strong diabatic heating along the ascending trajectories.

In general, LH contribution and heating are maximum along the mid-latitude baroclinic zone in the major storm track regions of the North Pacific, North Atlantic and Southern Ocean, and located slightly upstream of the maxima in blocking occurrence (Fig. 1).

The spatial relationship between LH and blocking intensification is shown in Fig. 5a,b, with the help of the spatial distribution of the location of strongest blocking intensification (white contours), as well as the intensification location of the 5% blocks with strongest (black crosses; 'moist' blocks) and weakest (gray crosses; 'dry' blocks) LH contribution [5% cases in the top (bottom) percentile of Fig. 4]. The location of maximum intensification of a block is defined as the point where the blocks upper-level anticyclonic PV anomaly (averaged over the blocking area) intensifies the most within a 12-h period along its track. It should be noted that the strongest intensification occurs for most blocks during onset: during the first 24 hours for 60% of all blocks, and during the first 48 h for 75% of all blocks. In general, preferred regions of blocking intensification are found off the east coast of North America extending into the North Atlantic and in the western and eastern North Pacific. Another confined maximum is found downstream of the Ural Mountains. In addition, blocks intensify over Northeast America and northern Asia in summer. In the SH, blocks intensify over the South Atlantic throughout the year and over the entire longitudinal band between 60°W to 90°E in DJF. Intensification frequencies are, however, low in the western South Pacific in JJA.

The spatial distribution and the seasonal progression of blocking intensification are in accordance with Rossby wave initiation climatology (Röthlisberger et al. 2018), again highlighting the dynamical link between blocking and transient eddies: Blocks preferably form over the ocean within the storm tracks in regions of strong LH contribution, pointing to an important influence of LH for the spatial distribution of blocking intensification and thus also genesis as most blocks intensify early in their life cycle. This influences the typical life cycle of blocks: They form in regions of strong LH (for example over the North Atlantic basin) and reach their maximum amplitude further downstream (over Europe), where wave breaking can occur. Subsequently, blocks typically propagate downstream into regions with weak LH contribution, where they decay. Exception is the confined region in the lee of the Ural mountains in DJF, where blocks intensify with minimum LH contribution. The interaction between

topography-forced planetary waves and downstream propagating wave trains emanating from the North Atlantic may contribute to the formation of blocking in this region with little diabatic heating (e.g., Luo et al. 2016). Some blocks over Europe and Australia during JJA can form with very small LH contribution (gray crosses in Fig. 5b). This is surprising considering that these regions are located at the eastern end of the ocean basins in the proximity of the climatological storm tracks. However, it has been shown by Nakamura et al. (1997), Michel and Rivière (2011) and Drouard and Woollings (2018) that blocking onset over Europe is frequently supported by an incoming quasi-stationary Rossby wave train extending from the subtropical western Atlantic. Likewise, blocking over Australia can be preceded by a Rossby wave train over the Indian Ocean (Risbey et al. 2018). This is consistent with our trajectory analysis that shows a substantial increase in LH contribution along an extended period of seven days for these regions (Fig. 4), suggesting that LH can initiate waves that propagate in regions with weaker LH contribution where blocking forms due to dry dynamics.

4.3 Evolution of latent heating during the blocking life cycle

The temporal tracking of individual blocking anticyclones gives further insight into the influence of LH on blocking during the different phases of the life cycle: onset (first day), decay (last day) and mature (days in between) phases. Figure 6 shows the median temporal evolution of the LH contribution, blocking intensity (average upper-level anticyclonic PV anomaly) and spatial extend for all 4270 blocks as a function of the blocking lifetime. The first (last) time step is defined as blocking genesis (decay). The temporal evolution of blocks typically follows a distinctive life cycle with onset (fast increase in size and intensity), mature (stabilization, almost constant size and intensity) and decay (relatively fast decrease in size and intensity) phases. A comparison of blocking size and intensity (Fig. 6b, c) indicates a relationship between these two characteristics with a Spearman rank correlation coefficient of − 0.68, i.e. more intense blocks (i.e., more pronounced upper-level PV anomalies) are typically also larger. The temporal development shows that the onset of blocks is characterized by a fast amplification of transient synoptic-scale waves into persistent large-amplitude blocks. The evolution of the median LH contribution (Fig. 6a) confirms that the importance of LH changes throughout the life cycle: it is largest during onset (60%) and than gradually declines to the lowest value (20%) when a block decays. This trend is associated with the (eastward) propagation of the blocks away from the localized heating source, where the strongest intensification during onset occurs, into regions with smaller LH contribution (see again

Fig. 6 **a** Percentage of trajectories with $\Delta\theta > 2$ K (%), **b** blocking intensity (pvu) (in SH multiplied with $-$ 1) and **c** spatial extent (km^2) as a function of blocking age. The x-axis is defined as the number of days since the first identification of a specific blocking event (left part), and the number of days before the decay of the block (right part). Black lines show the medians for all 4270 blocking events with interquartile range (25th–75th percentiles) in gray shading. Yellow (blue) lines show the mean for the 5% blocks with strongest (weakest) LH contribution (for each n = 213). In addition, examples for a dipole block (gray dashed lines) and an omega block (gray dotted lines) are shown. Magenta dots indicate the times of maxima in the LH contribution (LH bursts). Note the overlapping, as both example blocks have a lifetime shorter than 10 days
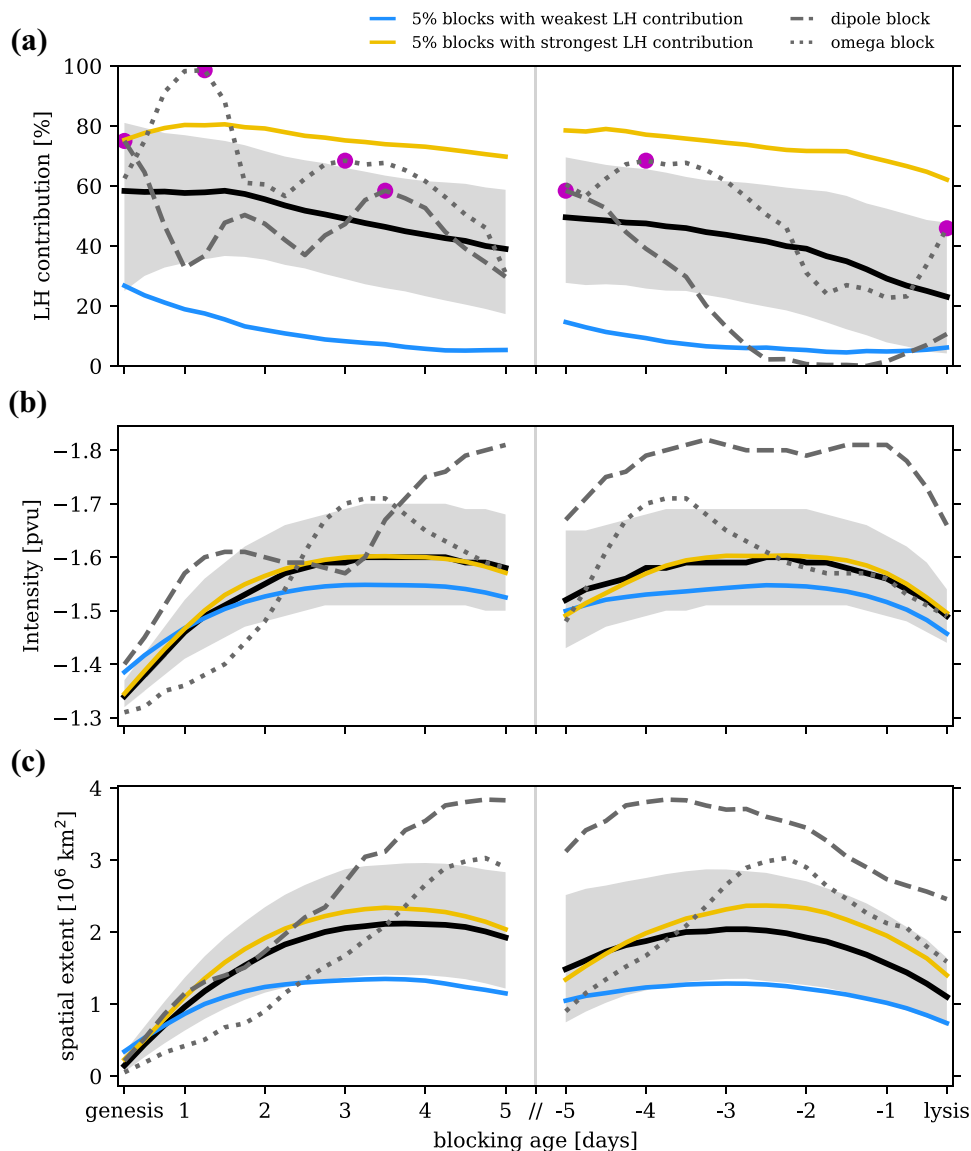

Fig. 5). At decay, 75% of all blocking trajectories have experienced a net cooling, and 10% of all blocking trajectories have already been recirculating in the blocking anticyclone for at least 3 days (not shown). A reduced LH contribution, the radiative decay of upper-level anticyclonic PV anomalies (Hoskins et al. 1985), and the equatorward migration of the system can lead to the dissipation of the blocking.

It has been shown in Sect. 4.2 that blocks can form with different LH contribution and that blocks dominated by moist-diabatic processes develop in different regions than those that are dominated by dry-adiabatic processes. Figure 6 shows that there are distinct differences also in other properties of the moist (5% blocks with strongest LH) and dry (5% with weakest LH) blocks. Moist blocks for which LH contribution is particularly strong throughout the development (yellow lines in Fig. 6) are on average more intense and larger than dry blocks (blue lines). In addition, moist

blocks are amplified more strongly during onset. However, also the dry blocks experience distinct LH contributions (> 20%) during genesis, highlighting the overall importance of LH for blocking onset.

The distributions (gray shading in Fig. 6) show that the variability between individual blocking events is substantial throughout the lifetime. While the median of many blocking events is characterized by a gradual evolution, individual blocking events experience multiple intensification phases and a fluctuation in size and intensity during their life cycle, as illustrated by two examples of blocking events over the North Atlantic and Europe (dipole block between 2 and 10 October 2016 with averaged LH contribution of 30.6%: gray dashed lines) and the North Pacific and North America (omega block between 28 April–5 May 2016 with averaged LH contribution of 57%: gray dotted lines). These fluctuations in intensity and size are often

preceded by bursts of LH (local maxima of LH contribution, see magenta dots in Fig. 6a). Note that these fluctuations in LH and blocking intensity/size do not correlate perfectly also owing to the lagged response of blocking to LH bursts. However, the examples illustrate that a block typically exhibits its most rapid amplification during a LH burst, and this intensification can be significantly magnified by an accumulation of such LH events (or a particularly large one). The examples show the episodic nature of LH during the blocking life cycle. Typically, a blocking event exhibits 2–3 LH bursts (average over all blocking events: 2.3 LH bursts), which are separated by periods of reduced LH contribution. Since the LH contribution varies strongly in time, the average LH contribution and the blocking lifetime are not correlated (Spearman rank correlation coefficient of − 0.07). However, for long-lived blocks with a lifetime of > 10 days, the number of LH bursts increases to 3–4 (in comparison to 1–2 LH bursts for short-lived blocks with < 10 days), which suggests that multiple LH bursts can extend the lifetime of a block.

The diabatic injection of (new) anticyclonic air during such LH bursts contributes not only to blocking onset, but also to the reinforcement and thus maintenance of the blocking anticyclone, which diminishes the tendency for dissipation. In the following, it is shown that these fluctuations in blocking characteristics are associated with the passage of synoptic-scale migratory eddies.

4.4 Origin of heating trajectories: the role of upstream cyclones

In the following, conditions during ascent and latent heat release in blocking air masses are analyzed in more detail. Fig. 7 shows the spatial distributions of trajectories affected by LH at the time of maximum heating (maximum positive $\Delta\theta$ in 6 h along the trajectories), highlighting the regions where the strongest LH occurs. From these regions, the trajectories ascend into the blocking anticyclones, leading to a strong linkage between the spatial patterns shown in Fig. 7 and the mean LH contribution to blocking (Fig. 5). The trajectory densities for both blocking indices (Fig. 7a, b, for APV and Fig. 7c, d for AGP) are shown, but only discussed for APV, as similar spatial patterns are obtained with the AGP blocking index.

In boreal winter over the NH, the blocking trajectories are heated diabatically and ascend mainly over the ocean, in particular over the North Pacific and the western part of the North Atlantic, whereas very few trajectories are heated over land. In summer, the LH occurs at all longitudes, also over continental areas, most prominently North America and Eurasia. In the SH, there is much less zonal and seasonal variability than in the NH, with a local maximum over the South Pacific during JJA, and weaker maxima over the South Atlantic and the South Indian Ocean. A small maximum of LH over land is found over Patagonia in austral summer. In both hemispheres, the strongest LH typically occurs at

Fig. 7 Spatial densities of blocking trajectories with $\Delta\theta >$ 2 K at the location of maximum latent heat release (maximum positive $\Delta\theta$ in 6 h) before arriving in a blocking region for **a, b** APV blocks and **c, d** AGP blocks during DJF (left) and JJA (right). Units are % $(10^6 \text{ km}^2)^{-1}$ and normalized for each hemisphere separately such that the spatial integral over each hemisphere yields 1. **a–d** Regions where the total APV (AGP) blocking frequency (≈ main blocking trajectory starting locations) is larger than 6% (4%) are shown by the magenta contours (see also Fig. 1)
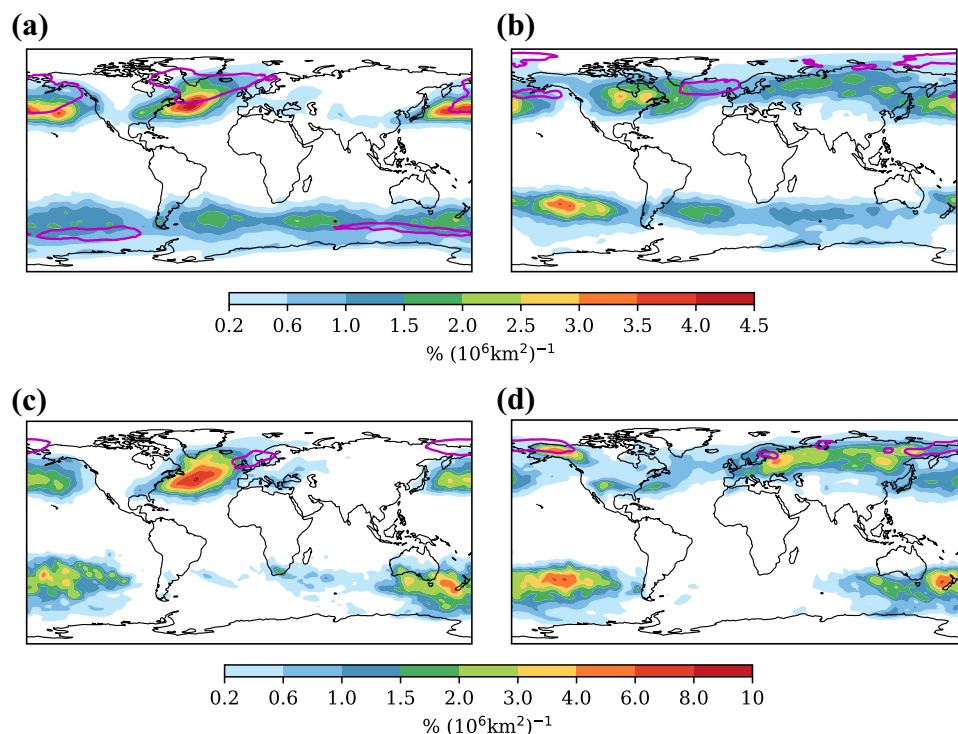
higher latitudes in summer than in winter, in line with the poleward contraction of the storm tracks in summer.

Overall, LH is highest along the mid-latitude baroclinic zone in the storm track regions. During winter, over the warm ocean currents (for example the warm Gulf stream in the western North Atlantic), the strong ocean-to-atmosphere heat fluxes (Aemisegger and Papritz 2018) and the enhanced storm track activity favor ascent of low-level moist air masses and latent heat release (Dacre and Gray 2009; Binder et al. 2016), whereas over land and at higher latitudes moisture supply is limited due to colder environmental conditions, leading to general weaker LH contribution to blocking. Over the eastern parts of the Atlantic and Pacific Oceans, the cyclones are located farther north (Fig. 1a), where moisture availability is limited (Pfahl et al. 2014), leading to less LH. The small local maximum in DJF in the southeastern United States is likely associated with lee cyclones (Wernli and Schwierz 2006) and moisture from the Gulf of Mexico. The spatial shift of the regions with high LH contribution towards the continents in summer is in good agreement with increased cyclone activity and surface evaporation, and thus moisture availability and uptake over land (see Fig. 2 in Pfahl et al. 2014). In summer, extratropical cyclones are typically weaker and less frequent compared to other seasons, which explains the lower LH contribution and blocking frequency over the North Atlantic and North Pacific during summer (Fig. 1b), despite increased temperature and atmospheric moisture content. In the SH, the seasonal cycle is not as clear as in the NH, as the mid-latitude storm track maintains its strength throughout the year. Also Quinting and Reeder (2017) have identified the mid-latitudes between South America and Australia as trajectory source regions of upper-level anticyclones over Australia. The equatorward shift of the LH regions (and blocking, see Fig. 1d) in the South Pacific during austral winter (JJA) is in line with the presence of a split jet east of Australia (Trenberth 1985).

Temporally, the strongest heating occurs at a median time between 1 and 2 days prior to the arrival in the block and at a location upstream and equatorward of the main blocking regions (magenta contours in Fig. 7a, b). For AGP blocks, which are located further away from the main LH regions (Fig. 7c, d), the time of strongest heating occurs at a median time between 2 and 3 days prior to the arrival in the block. These locations relative to the block are consistent with the findings of Lupo and Smith (1995), who found strongest cyclone deepening rates 36 h before blocking occurrence, that is when LH in the cyclone is at its peak intensity (see also Binder et al. 2016). As quantified in previous studies (Hawcroft et al. 2017), most of the latent heat release in the mid-latitudes occurs in association with extratropical cyclones in the WCB. Many aspects of the spatial and seasonal distribution in Fig. 7 is in good agreement with the climatological distribution of WCB ascent regions (Madonna

et al. 2014). For the blocking air masses in the heating regime, LH is strongest in the mid-troposphere at a median of 520 hPa, which is comparable to the level of strongest heating in WCB trajectories (Madonna et al. 2014). Interestingly, this typically happens when liquid cloud water freezes and water vapor is deposited onto ice crystals (see Fig. 7b in Madonna et al. 2014).

In order to further investigate the mechanism leading to diabatic heating and the cross-isentropic transport of the blocking air masses, the trajectories are used to identify environmental conditions during the time of strongest diabatic heating. Figure 8 shows composite maps of blocking trajectories with $\Delta\theta > 5$ K at the time of strongest diabatic heating along the trajectories for the NH. The coordinates are defined relative to the position of each individual blocking trajectory (yellow star at 0° longitude and latitude). Note that qualitatively similar composites are obtained for the SH and if all trajectories with $\Delta\theta > 2$ K are considered. When comparing the seasonal composites for NH blocking trajectories, it should be kept in mind that most LH occurs over sea at a median latitude of 40° N in DJF, but over land at a median latitude of 50° N in JJA (see Fig. 7).

The composites show that the ascent and LH of the air masses prior to reaching the block are related to an approaching mid-latitude upper-level PV trough and a surface cyclone (negative SLP anomaly at the leading edge of the trough) that typically occur prior to (temporal lag of 1–2 days) and upstream of blocking. This configuration corresponds to the classic picture of baroclinic development with a westward tilt with height between the low-level cyclone and the positive upper-level PV trough (e.g., Martin 2006). The low-level wind at 850 hPa indicates cyclonic circulation around the SLP minimum and a strong poleward low-level flow ahead of the cyclone, particularly in the transition zone between cyclonic and anticyclonic anomalies. This circulation contributes to the poleward advection of warm and moist air towards the mid-latitude baroclinic zone, where the air ascends along the poleward-sloping isentropes until condensation occurs, releasing latent heat. The location of the trajectories during maximum latent heat release lies in a region of anomalous high θ_e east of the cyclone center in the warm sector, just ahead of the upper-level trough, and hence in a region of upper-level forcing for ascent (see also Binder et al. 2016). θ_e values of the air masses affected by LH are substantially higher than in the surrounding air, with a median anomaly of 7.5 K compared to the monthly climatology at the same location. The 850-hPa θ_e patterns also indicate the existence of weak (as a result of the compositing) surface cold and warm fronts, denoting enhanced thermal advection.

The location of the trajectories also coincides with the peak precipitation near the cyclone center, where the air masses ascend over the surface warm front. Vertical
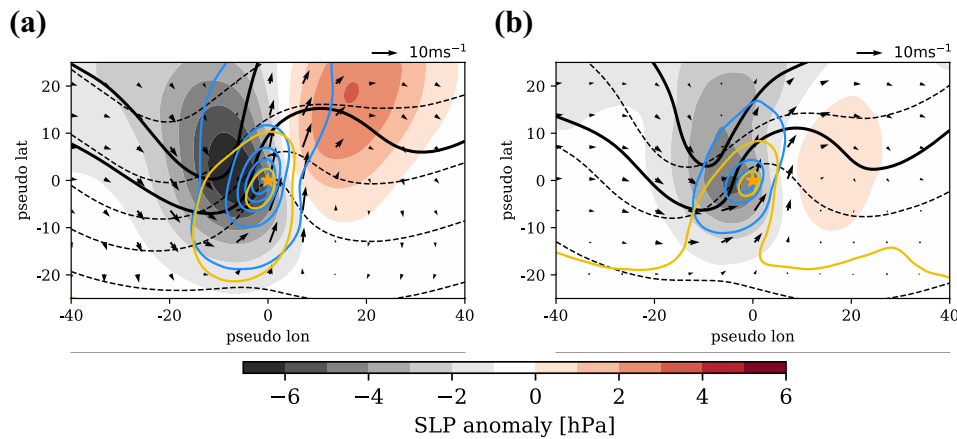
Fig. 8 Composite maps of NH blocking trajectories with $\Delta\theta > 5$ K at the time of maximum latent heat release along the trajectories for **a** DJF and **b** JJA. The yellow star indicates the position of the trajectories that is used as the center point for the composites. SLP anomaly (shading, hPa), upper-level PV (thick black contours for 2 and 3 pvu), θ_e on 850 hPa (black dashed contours every 10 K), wind on 850 hPa (black arrows, m s^{-1}), convective and large-scale precipitation (yellow and blue contours starting from 2 mm day^{-1} with interval of 4 mm day^{-1})

velocities are also at their maximum in this diabatic region of the composites (not shown). The south-westward extension of the precipitation band from the cyclone center is co-located with the location of the composite cold front. The large-scale precipitation (as obtained from the micophysics parameterization) band extends more to the north, while especially in JJA, convective precipitation (as obtained from the convection scheme) is also found in the southern part of the composite, probably formed in convective weather systems over the continents. In quantitative terms, large-scale precipitation is the dominant term with rates of up to 20 mm day^{-1} in DJF and 13 mm day^{-1} in JJA. The convective precipitation does not exceed 8 mm day^{-1}, however the relative contribution differs between winter (where trajectories are mostly located over sea) and summer (mostly over land): While in winter the majority of the precipitation is produced by the large-scale scheme, in summer ∼ 40% of the total mean precipitation is contributed by convection. The mean rain rates shown here are consistent with cyclone-centered composites in Booth et al. (2018). These findings indicate that convective processes ahead of an approaching upper-level trough, facilitated by the lower static stability underneath the trough (cf. Hoskins et al. 1985), could also represent a source of diabatically-heated blocking air masses. While the role of convective weather systems cannot be quantified with our trajectory-based approach, previous studies (Rodwell et al. 2013; Magnusson 2017) also point towards the importance of convective processes for errors in blocking predictions over Europe.

Downstream of the cloud-diabatically active region the composites indicate the development of the incipient block with an upper-level ridge and a high-pressure signature

at the surface. The cyclonic circulation transports the air masses towards the upper troposphere to the north and east of the cyclone. The resulting anticyclonic PV anomaly near the jet stream contributes to the subsequent blocking formation or maintenance.

The trajectory-centered composites used here are consistent with cyclone-centered composites shown in previous studies (e.g., Tamarin and Kaspi 2016; Binder et al. 2016), and main features of developing extratropical cyclones can be identified. The features are more pronounced in the DJF composite, because winter cyclones over sea are typically stronger. Note that our composites do also include cases of extratropical transition of recurving tropical cyclones (e.g., Riboldi et al. 2018) and low-level cyclonic PV anomalies that develop in the absence of upper-level forcing (Boettcher and Wernli 2013), both of which are known to modify the mid-latitude upper-level flow.

The trajectory analysis provides a synoptic perspective on the dynamical link between blocking and upstream baroclinic eddies in the storm track regions [the classical 'eddy-mean flow' interaction, e.g., Hoskins et al. (1983)]. The diabatic (and quasi-adiabatic) poleward transport of anticyclonic air masses into the blocking region occurs primarily on the eastward side of developing cyclones. Recalling the episodic nature of the LH contribution during the blocking life cycle described in Sect. 4.2 (see again Fig. 6), it should be emphasized that a series of transient cyclones and their associated cloud-diabatic processes, rather than a single primary cyclone, typically contribute to block formation and maintenance. For instance, in the case of the dipole block (gray dashed lines in Fig. 6), a rapidly intensifying cyclone initiated downstream ridge building and

the subsequent onset of the block (magenta dot at genesis), followed by a surface cyclone (Diabatic rossby wave, see again Boettcher and Wernli 2013) which further amplified the block (magenta dot at blocking age 3.5 days) and led to anticyclonic wave breaking over Europe. While blocking is a long-lived phenomena, the surrounding weather systems have usually a much more transient character. This cumulative action of groups of synoptic eddies in blocking formation, intensification and maintenance was also discussed in previous studies (Hoskins and Sardeshmukh 1987; Nakamura and Wallace 1993; Lupo and Smith 1995; Yamazaki and Itoh 2012a; Raveh-Rubin and Flaounas 2017; Maddison et al. 2019).

## 5 The impact of LH on blocking structure

In addition to the direct diabatic PV modification and the net cross-isentropic transport of anticyclonic PV air to the upper troposphere, LH can also have an indirect effect on the upper-level PV structure by amplifying the vertical motion, which results in an enhanced divergent outflow along the strong upper-level PV gradient associated with the tropopause and jet stream. When strong vertical and divergent motion impinges on the jet stream, a downstream Rossby wave amplification can be triggered (Davis et al. 1993; Teubler and Riemer 2016).

The effect of the divergent outflow associated with LH on the structure and development of blocking is evaluated here by calculating the PV advection by the divergent (irrotational) component ($\mathbf{v}_\chi \cdot \nabla PV$) of the full wind following Riemer et al. (2008), Archambault et al. (2013). The divergent wind is obtained via Helmholtz partitioning, using a successive overrelaxation method. In addition, the role of the non-divergent (rotational) wind component ($\mathbf{v}_\psi$) is investigated, which highlights the contribution of the balanced flow associated with the upper-level PV distribution. PV advection by the divergent and non-divergent wind is averaged vertically between 500 and 150 hPa to assess the flow component along the PV gradient at upper levels. The sum of these two flow components gives the PV advection by the total wind ($\mathbf{v}_\chi + \mathbf{v}_\psi$)·$\nabla PV$.

Blocking-centered composites are then constructed to reveal the relationship between blocking, surface cyclone, latent heating and upper-tropospheric divergence. The composites are averaged over the genesis (first day after the blocking onset), mature (one day centered on the time of peak intensity) and decay (last day before blocking decay) phases (Figs. 9, 10). For each block, a domain of approximately 40° around the block's center of mass (yellow star) is used. Note that these averages incorporate all 4270 blocks detected in the climatology, including mid-latitude and high-latitude blocks in both hemispheres. Hence, there is a high
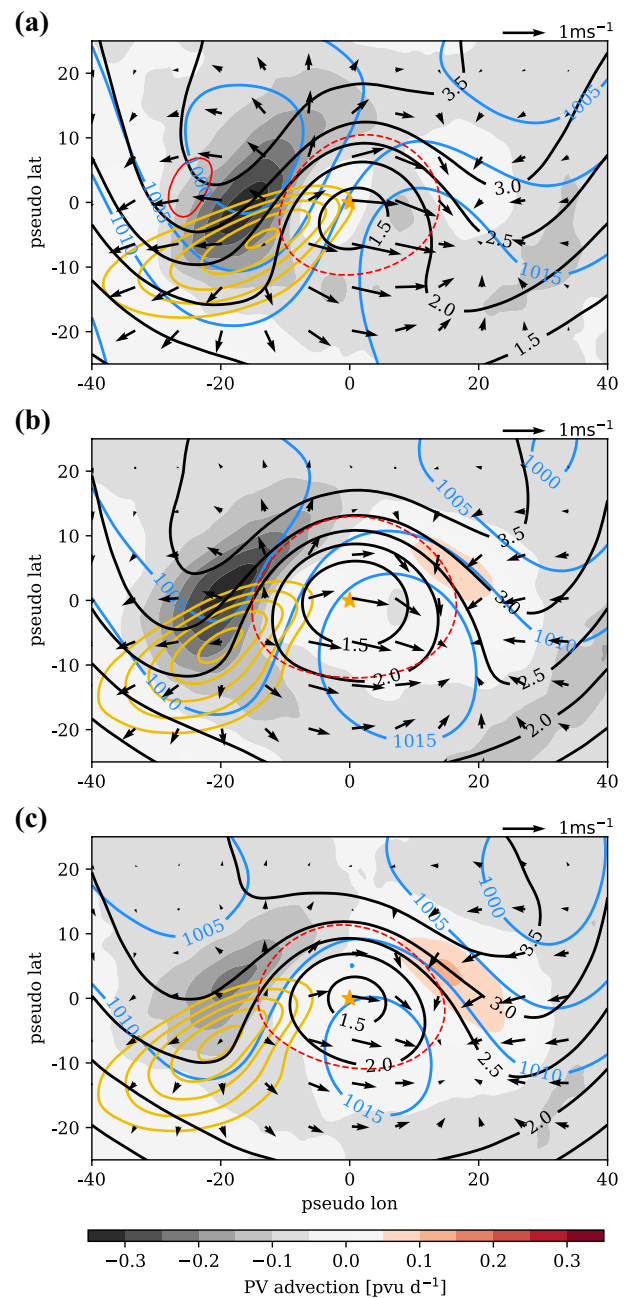
Fig. 9 Blocking-centered composite maps during **a** onset (first day after the blocking onset), **b** mature (one day centered on the time of peak intensity) and **c** decay (last day before blocking decay) phases. Upper-level PV (pvu, black contours), upper-level divergent wind vectors of the full wind (m s^{-1}; reference vector in upper right), upper-level PV advection by the divergent component of the full wind (pvu day^{-1}, shading), frequency of trajectories with $\Delta\theta > 2$ K in three days at the time of maximum heating (yellow contours from 0.06 to 0.2% every 0.02; note that there is a time lag of median -1.5 days between maximum LH and the time of the composites), upper-level PV anomaly [pvu, red contours for -0.5 (dashed) and 0.5] and SLP (hPa, blue contours). All blocking composites in this study are presented in poleward-oriented format, meaning that SH blocks are flipped meridionally. PV values in the SH have been multiplied by -1
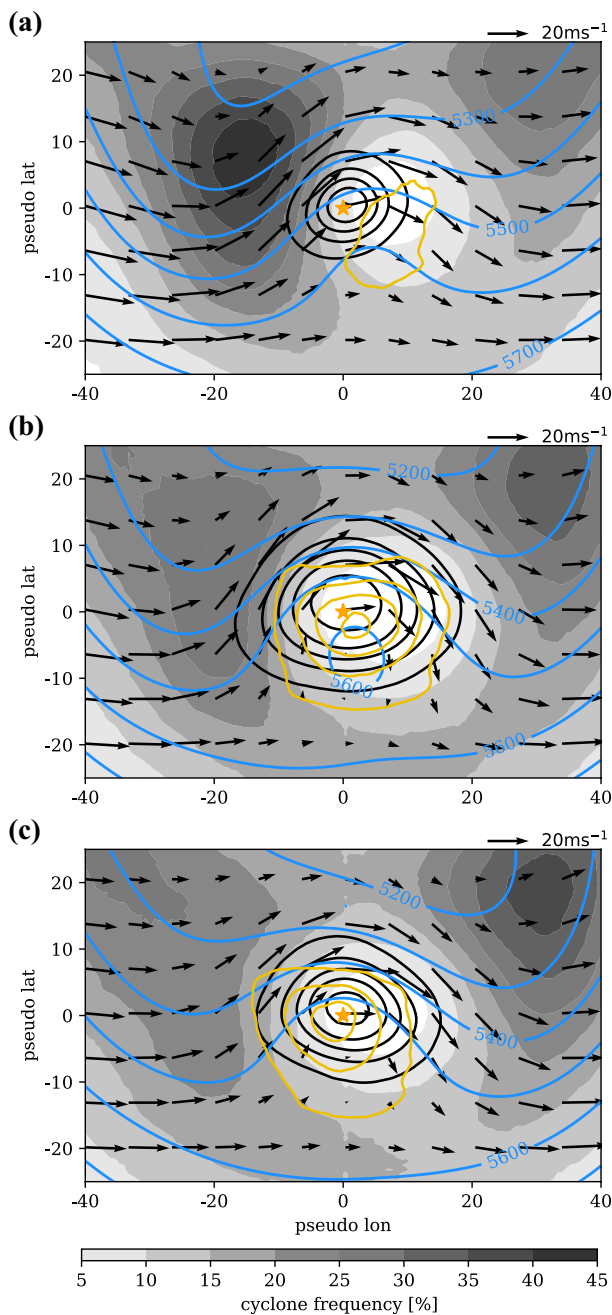
Fig. 10 Blocking-centered composite maps during **a** onset, **b** mature and **c** decay phases. Z500 geopotential height (m, blue contours), upper-level wind vectors (m s^{-1}; reference vector in upper right), cyclone frequency (%, shading), APV blocking frequency (black contours, 10–90% every 20) and AGP blocking frequency (yellow contours, starting from 2% every 2)

case-to-case variability (different blocking sizes and shapes) and finer structures are smoothed out due to disparate locations relative to the blocking center. The position of extratropical cyclones and AGP blocks relative to the APV blocking is shown in the composites in Fig. 10.

Generally, the composites show the main characteristics of blocking, i.e. a marked poleward displacement of upper-level PV (black contours in Fig. 9) and Z500 (blue contours in Fig. 10) contours around the blocking center (yellow star) with an anticyclonic rotation (Fig. 10). Note that these signals are vertically extended (averaged between 150 and 500 hPa) and include omega-shaped (more frequent in the North Pacific and SH) and dipole-shaped (more frequent in the North Atlantic) blocks. The composite structure is similar to a large-scale ridge during genesis, and the poleward intrusion of low-PV air that is surrounded by high-PV air becomes more pronounced in the mature and lysis composites where the 2-pvu contour (and Z500 contours) overturns (closed 2-pvu contours), resulting in an inversion of the meridional PV gradient south of the blocking center, a signal of wave breaking. The negative PV anomalies (Fig. 9) and the APV blocking frequency (Fig. 10) show that the spatial extent of the block is largest during the mature phase.

The evolution of the block shows a more baroclinic structure during onset with a westward tilt between the SLP maximum and the upper-level PV ridge (Fig. 9). The composites become more barotropic with blocking age. The surface anticyclone (closed SLP contours) located below the negative PV anomaly is strongest as the block reaches maximum intensity (mature phase, Fig. 9b). Most evident during the mature phase, the block is most intense and locally decelerates and reverses the mean westerly flow and splits the jet stream with a strong northerly (maximum wind speeds up to 30 m s^{-1}) and a weaker southerly branch around the block (Fig. 10b), contributing to a large-scale deformation flow to the southwest where Z500 (and PV) contours deviate, which follows the original description of Rex (1950). AGP blocking frequencies are small during onset, but increase drastically when the block reaches maturity and wave breaking occurs. AGP blocks are located southeast of the APV blocking during onset, where anticyclonic overturning and flow reversal is expected (Altenhoff et al. 2008), and south of the APV block during the mature phase. The rather low values of AGP blocking frequencies are due to averaging over many regions where AGP blocks are rare, including the SH and mid-latitude North Pacific.

On both sides of the block, PV troughs are present (see again Fig. 9), which is indicative of wave activity. Upstream of the blocking, a SLP minimum below the trough indicates the presence of cyclones, most prominently during onset, highlighting the role of upstream cyclones as precursor to blocking. During onset, the cyclone frequency maximum (Fig. 10a) is located to the northwest of the block, and the area of enhanced cyclone frequency extends to the north and southwest of the block. The vast majority of blocks are accompanied by one or more cyclones during their lifetime, and the large standard deviation of the cyclone frequency in the composites is an indication of a strong case-to-case

variability in the exact location and occurrence of these upstream cyclones (not shown). While most cyclones are located upstream of the block during strongest interaction, i.e., during a LH burst, this frequency pattern indicates that some cyclones have already propagated pole- and equatorward around the block. Upstream cyclone frequency gradually declines during the blocking lifecycle, a development consistent with the temporal evolution of the LH contribution (Fig. 6a). According to Berggren et al. (1949) and Shutts (1983), a diffluent flow can slow down and amplify approaching synoptic-scale waves, which provides favorable conditions for large-scale poleward transport of anticyclonic air masses into the block (so-called eddy-straining mechanism, see Shutts 1983). The synoptic setup shown here in the composite maps is consistent with previous work that found synoptic eddies embedded in a diffluent flow to strengthen the blocking. Downstream cyclones, not further discussed in this study, are present during the entire blocking lifetime, and their frequency slightly increases with blocking age, a sign of downstream wave development.

Independent of blocking age, the ascending air masses affected by LH (yellow contours in Fig. 9) are located below the western flank of the blocking, just below the leading edge of the upstream trough (cf. Sect. 4.3). Accordingly, intense divergent outflow (Fig. 9) is located above the cloud-diabatic region on the western flank of the blocking, where the strongly ascending air masses reach the upper troposphere and spread out horizontally. The divergent outflow is strongest during onset and weakens with blocking age, in line with the temporal evolution of the LH contribution (Fig. 6a). A region of convergence is found on the eastern flank of the blocking ridge, where subsidence is expected. The divergent outflow is located on the equatorward side of the jet and has a component along the PV gradient towards the pole. Therefore, it advects anticyclonic PV poleward. The jet stream is shifted in the same direction and locally accelerates.

This negative PV advection by the divergent wind (Fig. 9) on the western flank leads to a westward (and poleward)

expansion of the blocking anomaly. Conversely, positive PV advection opposes ridge building on the eastern flank. The magnitude of the negative PV advection in the composites is similar during the onset and mature phases ($-0.35\,\mathrm{pvu\,day^{-1}}$), whereas the positive PV advection on the eastern flank is weaker throughout the blocking lifecycle ($+0.1\,\mathrm{pvu\,day^{-1}}$). This asymmetric configuration between negative and positive PV advection during onset and mature phase promotes the amplification and zonal widening of the blocking region. The pattern of the PV advection changes substantially during the decay stage, with a much weaker negative PV advection on the western flank of roughly the same magnitude as the positive PV advection on the eastern flank, resembling a more symmetric configuration. This is a result of the reduced divergent outflow during the decay of the block. Note that, in addition to LH, the PV advection by the divergent wind is also related to the strength of the upper-level PV gradient, which explains the comparable magnitude of negative PV advection in spite of reduced divergent wind (and LH) during the mature phase compared to onset. The ongoing advection of low-PV air during the onset and mature phases extends the ridge not only poleward, but even more to the west. This contributes to the amplification and quasi-stationary behavior of blocking, as it counteracts the dissipation and eastward movement due to the mean westerly flow. This westerly flow manifests itself in a positive PV advection by the non-divergent wind (Fig. 11b; with maximum values of $+1.25\,\mathrm{pvu\,day^{-1}}$), i.e. it advects the block eastward, which overcompensates the negative PV advection by the divergent wind. In general, the divergent wind is one order of magnitude smaller than the non-divergent wind, however, the PV advection by the two wind components is of much more comparable magnitude since the divergent wind projects directly onto the PV gradient. The total (rotational plus divergent) wind still advects the block downstream, albeit with a reduced velocity compared to the mean flow (see again Fig. 2). The role of the divergent wind for keeping blocks stationary was also noted by Mullen (1987).

Fig. 11 Same as Fig. 9a but **a** PV advection by the divergent wind based on diagnostically calculated vertical motion from the quasi-geostrophic omega equation and **b** PV advection by the non-divergent (rotational) component of the full wind during blocking onset. Note the different ranges of the colorbar
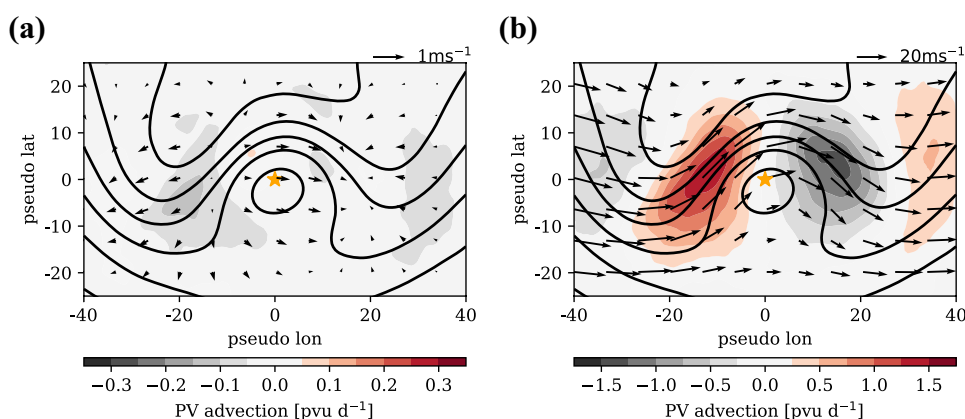
The Helmholtz partitioning used here to decompose the wind into divergent and non-divergent wind components does not provide information on the cause of the divergent outflow, that is, whether it is an indirect effect of LH or related to the dry, ageostrophic circulation of the large-scale balanced flow (e.g., Martin 2006). Following Graf et al. (2016), we employ the quasigeostrophic (QG) framework, based on the QG ω-equation in Trenberth (1978), to estimate the dry-dynamical adiabatic large-scale forcing for vertical motion and the associated upper-level divergence as compared to the diabatically driven outflow. We compute the divergence related to the QG ω via the continuity equation on pressure levels between 500 and 150 hPa. Figure 11a shows the blocking-centered composite during onset with the upper-level divergent wind obtained from the QG ω-equation. The QG forced divergent wind and its PV advection on the western flank are much weaker than the negative PV advection by the divergent outflow of the full wind. Dry QG dynamics account for roughly one third of the negative PV advection observed in the composites with the full vertical motion. Convergence and PV advection on the eastern flank of the block and ahead of the downstream trough are, however, not substantially reduced. The results are consistent with the findings of Quinting and Jones (2016) for the diabatic outflow of recurring tropical cyclones. Given the strong divergent outflow and the observed asymmetry in the PV advection by the divergent wind between western and eastern flank in the full wind composites (Fig. 9), it is clear that LH in the upstream cyclone significantly enhances the divergent outflow. While the large-scale dry-dynamical forcing from the upstream trough is essential for the ascent of the air masses into the blocking region (see Sect. 4.3), it does not explain the strong divergent outflow of the full wind and its impact on the blocking. We hence conclude that moist-diabatic processes and the associated LH in the mid troposphere strongly enhance the divergent outflow, and the succeeding interaction with the upper-level PV gradient modifies the amplification and propagation of blocking compared to the behavior expected from a purely dry QG perspective.

5.1 Difference between moist and dry blocks

Since blocks can form with different LH contributions (Sect. 4.2) and show significant differences in their development (Sect. 4.3), composite maps are compiled separately for the 5% blocks with strongest (moist blocks) and weakest (dry blocks) LH contribution in Fig. 12. Interestingly, the composites indicate a distinct structural difference. In the moist block composites (Fig. 12a, c, e), the PV pattern has a Ω-shape structure with a northwest-southeast tilt, in particular during the latter stages of development, which promotes cyclonic wrap up of the upstream trough,

suggesting that the intense LH and diabatic outflow in these blocks may favor cyclonic wave breaking. In addition, the cross-isentropic transport of low-PV within ascending airstreams reduces the upper-level PV in the center of the block and strengthens its anticyclonic anomaly (in comparison to the dry block composites), which peaks during the mature phase. For the dry blocks (Fig. 12b, d, f), the composite shows a cut-off low-PV anomaly already during onset, which is cut off from its tropospheric source and surrounded by high-PV stratospheric air. Anticyclonic wave breaking at the downstream flank becomes visible during the mature phase, setting up a dipolar configuration with a low-over-high PV anomaly during the mature phase of the development. This dipolar pattern counters the (weak) background westerly flow, keeping the block quasi-stationary without the diabatic outflow. Interestingly, without strong cloud-related LH and diabatic PV modification, the upper-level PV in the center of the dry blocks does not decrease during the life cycle. The cut-off blocks are likely to be residues of Rossby wave breaking (Pelly and Hoskins 2003a). Although Rossby wave breaking can evolve due to dry baroclinic dynamics alone (McIntyre and Palmer 1983), Zhang and Wang (2018) showed that upstream diabatic heating can help to amplify the upper-level ridge and subsequent wave breaking. This is consistent with our trajectory analysis, which shows a moderate LH contribution of 20% during onset for the dry blocks (Fig. 6a) and a substantial increase in LH contribution along an extended period of seven days (not shown). Again, this significant differences in the upper-level outflow and PV advection between the moist and dry blocks points to the importance of LH for vertical motion and the associated modification of the blocking structure.

In addition to the role of LH for the blocking structure, general statements about the geographical background flow can be made because the location of these blocks are in well-defined areas. It has been shown in Fig. 5a, b that blocks with maximum LH contribution typically develop in different regions compared to those with minimum LH contribution. Moist blocks are typically found within the main storm track regions of the North Pacific, western North Atlantic and eastern South Pacific, whereas dry blocks are located downstream, or on the equatorward flank, of the storm tracks over Europe, Asia and Australia. In this regard, our results are consistent with previous studies (Berrisford et al. 2007; Tyrlis and Hoskins 2008a; Altenhoff et al. 2008; Masato et al. 2012) who showed that a block's location relative to the climatological storm tracks is also important for the structure of the blocking, with mostly cyclonic wave breaking occurring on the poleward flank, and anticyclonic wave breaking on the equatorward flank of the storm track. The upstream and downstream zone of enhanced PV gradient in the moist block composites indicates that moist blocks from in a region of strong westerly winds. Our findings

Fig. 12 Blocking-centered composite maps during **a**, **b** onset, **c**, **d** mature and **e**, **f** decay phases for **a**, **c**, **e** 5% blocks with strongest LH contribution and **b**, **d**, **f** 5% blocks with weakest LH contribution. Upper-level PV (pvu, black contours), upper-level divergent wind vectors of the full wind (m s^{-1}; reference vector in upper right) and PV advection by the divergent component of the full wind (pvu day^{-1}, shading). Note the difference in PV advection color scale compared to previous figure
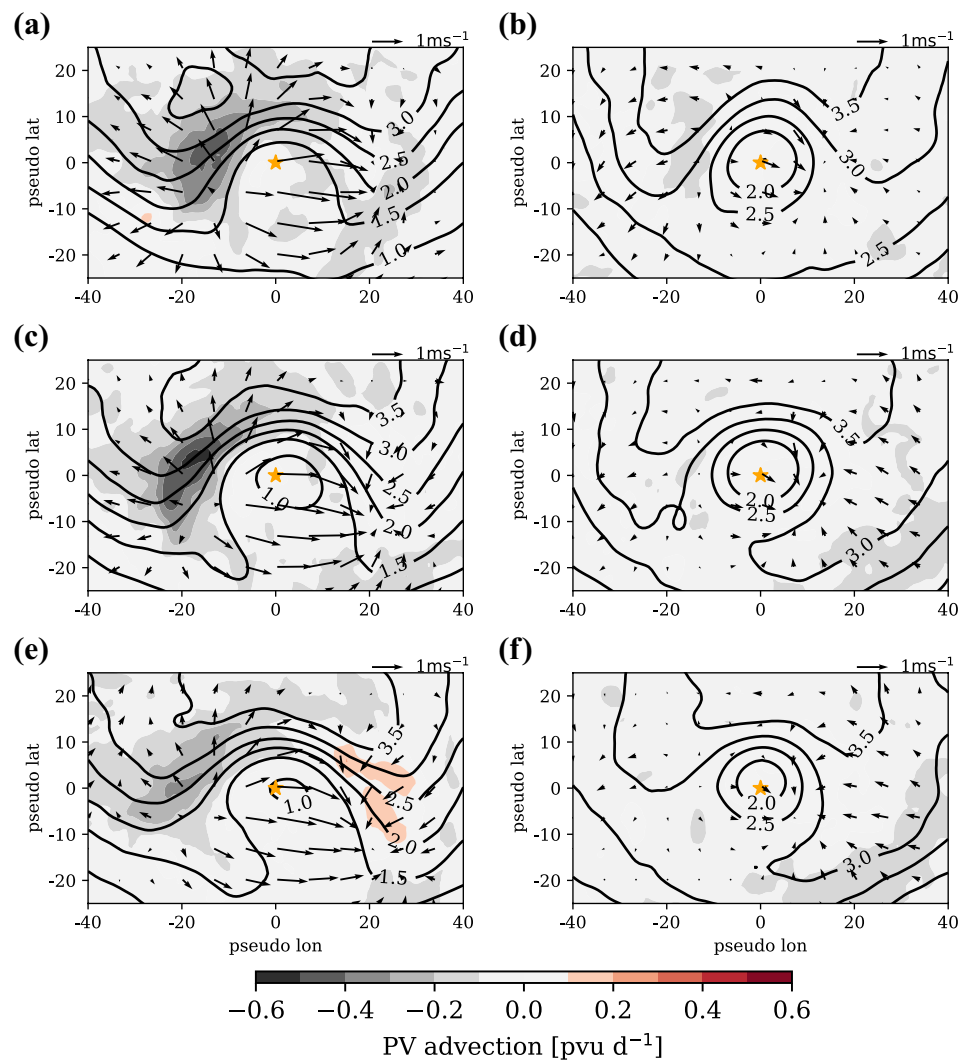
thus suggest that intense diabatic outflow provides the required flow amplification for perturbing the strong zonal jet and for keeping the blocks quasi-stationary. In contrast, dry blocks develop in regions where the zonal winds are weaker (reduced upstream and downstream PV gradients), which provides a more favourable environment for blocking initiation.

6 Conclusions

The present study explores the variability and dynamics of atmospheric blocking with a special focus on the role of moist-diabatic processes, in particular the release of latent heat in ascending airstreams, and discusses the importance of diabatic processes for the formation and maintenance of blocking in comparison to classical (dry-dynamical) blocking theories. We have compiled a comprehensive global climatology of blocking from the ERA-Interim dataset for

the period 1979–2016 to examine the seasonal and regional relationship between atmospheric blocking, extratropical cyclones, latent heating (LH) and the associated dynamical processes from a combined Eulerian (composites) and Lagrangian (air parcel trajectories) perspective. In order to capture a representative sample of different blocking flow patterns, blocking has been identified using two different blocking indices based on upper-level anticyclonic PV anomalies (Schwierz et al. 2004) and the reversal of the Z500 gradient (Scherrer et al. 2006).

The climatological trajectory analysis reveals that two different processes contribute to a block's anticyclonic PV anomalies: moist-diabatic processes with cross-isentropic transport of anticyclonic PV air (heating regime) and quasi-adiabatic processes with nearly isentropic transport of mostly anticyclonic PV air (no-heating "cooling" regime). Between 31 and 46% (58–67%) of all blocking air masses have been heated by more than 2 K, with a median heating of 8.5 K (12.5 K), during the final 3 (7) days before entering

the blocking anticyclone. These results corroborate earlier studies (Pfahl et al. 2015; Quinting and Reeder 2017) and highlight the fundamental importance of moist-diabatic processes for atmospheric blocking.

In agreement with classical blocking theories, the no-heating regime corresponds (i) to the mechanism proposed by Yamazaki and Itoh (2012a), according to which the blocking anomaly is maintained by selectively absorbing other synoptic-scale transient anticyclones or (ii) to the poleward quasi-adiabatic transport of (subtropical) air from lower latitudes ahead of extratropical cyclones (e.g., Shutts 1983; Colucci 1985) or during Rossby wave breaking (Pelly and Hoskins 2003a). These air masses experience weak diabatic cooling of a few K, probably caused by long-wave radiation, which may weaken the upper-level anticyclone (Hoskins et al. 1985). Further investigation is needed to quantify the role of long-wave radiation for blocking dissipation.

Temporal and spatial variability of blocking occurrence and intensification can be linked to cloud-diabatic activity. Blocking over the ocean, linked to strong ocean-to-atmosphere heat fluxes and enhanced storm track activity, is typically dominated by moist-diabatic processes throughout the year, whereas continental blocks exhibit strong seasonality with a minimum in diabatic contribution during winter, when moisture supply is limited. In general, moist-diabatic blocks develop faster than dry-adiabatic blocks, and are more intense and larger in extent. However, the large case-to-case variability of the diabatic contribution demonstrates that some blocks can also amplify in the absence of LH, and that different mechanism can dominate in different cases.

Futhermore, moist-diabatic processes are more important during blocking onset, which is characterized by rapid amplification of synoptic-scale ridges, and reduce to a minimum during the decay phase. Multiple episodes of increased LH contribution (LH bursts) during the blocking life cycle systematically precede blocking (re-)intensification and growth. This indicates that LH can contribute to both the high- (fast onset and fluctuation in intensity and size) and low-frequency (persistence and quasi-stationarity during maturation phase) properties of blocking anticyclones through the episodic injection of anticyclonic PV air and the reinforcement of the anticyclonic PV anomalies in the upper troposphere.

With the help of detailed composite and trajectory analyses, we have elucidated the chain of synoptic-scale processes involved in blocking formation and the specific role of LH. Air masses typically ascend into the blocking region ahead of an extratropical cyclone over a mid-latitude baroclinic zone. Forcing for ascent is incipiently provided by an approaching upper-level through, and if there is sufficient supply of moisture, this upper-level forcing triggers strong latent heat release that enhances the upward motion. This diabatically amplified ascent (often called warm conveyor belt) injects anticyclonic PV air into the upper troposphere and creates strong divergent outflow on the western flank of the block. Negative PV advection by the divergent outflow extends the blocking ridge westward, anchoring the block in place and slowing down its eastward progression. As a consequence, upstream cyclones are also slowed down and amplify meridionally when approaching the large-scale deformation flow to the southwest of the block, which allows subtropical air masses with anticyclonic PV values to travel a long way polewards within the blocking region, as described by Berggren et al. (1949) and Shutts (1983), among others. Hence, moist-diabatic processes do not operate in isolation but instead the interplay of a strong baroclinic wave, upper-level QG forcing for ascent and an intense, diabatically produced outflow highlights the importance of both dry and moist dynamics for blocking. Our findings thus complement the large body of previous work that found synoptic eddies to strengthen blocking.

As cyclones occur more frequently than blocking, a question that is still open is which cyclones initiate a blocking and which do not, and it is not clear whether cyclones with stronger diabatic heating are more likely to cause blocking. Pelly and Hoskins (2003a) have shown that an anomalous blocked flow is easier to maintain than to initiate, which points to an important role of the large-scale flow to provide a favourable environment to be prone to blocking initiation. Our blocking-centered composites show that the dynamical tropopause and the large-scale flow are already in an amplified state during blocking onset, which indicates that a large-scale open ridge was present prior to blocking onset. An anomalously diffluent flow prior to blocking onset was also pointed out by Colucci (2001), and recently Röthlisberger et al. (2018) highlighted the general relevance of a preexisting ridge for the initiation and growth of synoptic-scale waves. These findings reveal that the interaction between and phasing of planetary-scale flow anomalies and mobile synoptic-scale eddies plays an important role for blocking formation (Nakamura et al. 1997; Luo et al. 2014), and diabatic processes can provide the required flow amplification in addition to dry-dynamical forcing.

References

Aemisegger F, Papritz L (2018) A climatology of strong large-scale ocean evaporation events. Part I: identification, global distribution, and associated climate conditions. J Clim 31(18):7287–7312

Altenhoff AM, Martius O, Croci-Maspoli M, Schwierz C, Davies HC (2008) Linkage of atmospheric blocks and synoptic-scale Rossby waves: a climatological analysis. Tellus A 60(5):1053–1063

Archambault HM, Bosart LF, Keyser D, Cordeira JM (2013) A climatological analysis of the extratropical flow response to recurving western north pacific tropical cyclones. Mon Weather Rev 141(7):2325–2346

Barnes EA, Screen JA (2015) The impact of Arctic warming on the midlatitude jet-stream: Can it? Has it? Will it? Wiley Interdiscip Rev Clim Change 6(3):277–286

Barnes EA, Slingo J, Woollings T (2012) A methodology for the comparison of blocking climatologies across indices, models and climate scenarios. Clim Dyn 38(11):2467–2481

Barriopedro D, García-Herrera R, Trigo RM (2010) Application of blocking diagnosis methods to general circulation models. Part I: a novel detection scheme. Clim Dyn 35(7):1373–1391

Berggren R, Bolin B, Rossby C-G (1949) An aerological study of zonal motion, its perturbations and break-down. Tellus 1(2):14–37

Berrisford P, Hoskins BJ, Tyrlis E (2007) Blocking and Rossby wave breaking on the dynamical tropopause in the Southern Hemisphere. J Atmos Sci 64(8):2881–2898

Binder H, Boettcher M, Joos H, Wernli H (2016) The role of warm conveyor belts for the intensification of extratropical cyclones in Northern Hemisphere winter. J Atmos Sci 73(10):3997–4020

Boettcher M, Wernli H (2013) A 10-yr climatology of diabatic rossby waves in the Northern Hemisphere. Mon Weather Rev 141:1139–1154

Booth JF, Dunn-Sigouin E, Pfahl S (2017) The relationship between extratropical cyclone steering and blocking along the North American east coast. Geophys Res Lett 44(23):11,976–11,984

Booth JF, Naud CM, Willison J (2018) Evaluation of extratropical cyclone precipitation in the North Atlantic basin: an analysis of ERA-Interim, WRF, and two CMIP5 models. J Clim 31(6):2345–2360

Buehler T, Raible CC, Stocker TF (2011) The relationship of winter season North Atlantic blocking frequencies to extreme cold or dry spells in the ERA-40. Tellus A 63(2):212–222

Chang EKM, Yu DB (1999) Characteristics of wave packets in the upper troposphere. Part I: Northern Hemisphere Winter. J Atmos Sci 56(11):1708–1728

Charney JG, DeVore JG (1979) Multiple flow equilibria in the atmosphere and blocking. J Atmos Sci 36(7):1205–1216

Cheung HN, Zhou W, Shao Y, Chen W, Mok HY, Wu MC (2013) Observational climatology and characteristics of wintertime atmospheric blocking over Ural-Siberia. Clim Dyn 41(1):63–79

Colucci SJ (1985) Explosive cyclogenesis and large-scale circulation changes: implications for atmospheric blocking. J Atmos Sci 42(24):2701–2717

Colucci SJ (2001) Planetary-scale preconditioning for the onset of blocking. J Atmos Sci 58(8):933–942

Croci-Maspoli M, Davies HC (2009) Key dynamical features of the 2005/06 European winter. Mon Weather Rev 137(2):664–678

Croci-Maspoli M, Schwierz C, Davies HC (2007) A multifaceted climatology of atmospheric blocking and its recent linear trend. J Clim 20(4):633–649

Dacre HF, Gray SL (2009) The spatial distribution and evolution characteristics of North Atlantic cyclones. Mon Weather Rev 137(1):99–115

Davini P, D'Andrea F (2016) Northern Hemisphere atmospheric blocking representation in global climate models: twenty years of improvements? J Clim 29(24):8823–8840

Davini P, Cagnazzo C, Fogli PG, Manzini E, Gualdi S, Navarra A (2014) European blocking and Atlantic jet stream variability in the NCEP/NCAR reanalysis and the CMCC-CMS climate model. Clim Dyn 43(1):71–85

Davis CA, Stoelinga MT, Kuo Y-H (1993) The integrated effect of condensation in numerical simulations of extratropical cyclogenesis. Mon Weather Rev 121(8):2309–2330

Dee DP, Uppala SM, Simmons AJ, Berrisford P, Poli P, Kobayashi S, Andrae U, Balmaseda MA, Balsamo G, Bauer P, Bechtold P, Beljaars ACM, van de Berg L, Bidlot J, Bormann N, Delsol C, Dragani R, Fuentes M, Geer AJ, Haimberger L, Healy SB, Hersbach H, Hólm EV, Isaksen L, Kållberg P, Köhler M, Matricardi M, Mcnally AP, Monge-Sanz BM, Morcrette JJ, Park BK, Peubey C, de Rosnay P, Tavolato C, Thépaut JN, Vitart F (2011) The ERA-Interim reanalysis: configuration and performance of the data assimilation system. Q J R Meteorol Soc 137(656):553–597

Dole RM (1986) The life cycles of persistent anomalies and blocking over the north pacific. Adv Geophys 29(C):31–69

Dole RM, Gordon ND (1983) Persistent anomalies of the extratropical Northern Hemisphere wintertime circulation—structure. Mon Weather Rev 111:1567–1586

Drouard M, Woollings T (2018) Contrasting mechanisms of summer blocking over western Eurasia. Geophys Res Lett 45(21):12,12–40,48

Ferreira AP, Castanheira JM, Gimeno L (2016) Water vapour stratification and dynamical warming behind the sharpness of the Earth's midlatitude tropopause. Q J R Meteorol Soc 142(695):957–970

Graf MA, Wernli H, Sprenger M (2016) Objective classification of extratropical cyclogenesis. Q J R Meteorol Soc 143(703):1047–1061

Grams CM, Wernli H, Böttcher M, Čampa J, Corsmeier U, Jones SC, Keller JH, Lenz C-J, Wiegand L (2011) The key role of diabatic processes in modifying the upper-tropospheric wave guide: a North Atlantic case-study. Q J R Meteorol Soc 137(661):2174–2193

Green JSA (1977) The weather during July 1976: Some dynamical consideration of the drought. Weather 32(4):120–126

Hassanzadeh P, Kuang Z, Farrell BF (2014) Responses of midlatitude blocks and wave amplitude to changes in the meridional temperature gradient in an idealized dry GCM. Geophys Res Lett 41(14):5223–5232

Hawcroft M, Dacre H, Forbes R, Hodges K, Shaffrey L, Stein T (2017) Using satellite and reanalysis data to evaluate the representation of latent heating in extratropical cyclones in a climate model. Clim Dyn 48(7):2255–2278

Hoskins BJ, Karoly DJ (1981) The steady linear response of a spherical atmosphere to thermal and orographic forcing. J Atmos Sci 38(6):1179–1196

Hoskins BJ, Sardeshmukh PD (1987) A diagnostic study of the dynamics of the Northern Hemisphere winter of 1985–86. Q J R Meteorol Soc 113(477):759–778

Hoskins BJ, James IN, White GH (1983) The shape, propagation and mean-flow interaction of large-scale weather systems. J Atmos Sci 40(7):1595–1612

Hoskins BJ, McIntyre ME, Robertson AW (1985) On the use and significance of isentropic potential vorticity maps. Q J R Meteorol Soc 111(466):877–946

Ioannidou L, Yau MK (2008) A climatology of the Northern Hemisphere winter anticyclones. J Geophys Res Atmos 113(D8):D08119

Kuo Y-H, Shapiro MA, Donall EG (1990) The interaction between baroclinic and diabatic processes in a numerical simulation of a rapidly intensifying extratropical marine cyclone. Mon Weather Rev 119(2):368–384

Lejenäs H (1984) Characteristics of southern hemisphere blocking as determined from a time series of observational data. Q J R Meteorol Soc 110(466):967–979

Lejenäs H, økland H (1983) Characteristics of northern hemisphere blocking as determined from a long time series of observational data. Tellus A 35 A(5):350–362

Luo D, Cha J, Zhong L, Dai A (2014) A nonlinear multiscale interaction model for atmospheric blocking: the eddy-blocking matching mechanism. Q J R Meteorol Soc 140(683):1785–1808

Luo D, Xiao Y, Diao Y, Dai A, Franzke CLE, Simmonds I (2016) Impact of Ural blocking on winter warm Arctic—cold Eurasian anomalies. Part II: the link to the North Atlantic oscillation. J Clim 29(11):3949–3971

Lupo AR, Smith PJ (1995) Climatological features of blocking anticyclones in the Northern Hemisphere. Tellus A 47(4):439–456

Maddison JW, Gray SL, Martínez-Alvarado O, Williams KD (2019) Upstream cyclone influence on the predictability of block onsets over the Euro-Atlantic region. Mon Weather Rev 147(4):1277–1296

Madonna E, Wernli H, Joos H, Martius O (2014) Warm conveyor belts in the ERA-Interim Dataset (1979–2010). Part I: climatology and potential vorticity evolution. J Clim 27:3–26

Magnusson L (2017) Diagnostic methods for understanding the origin of forecast errors. Q J R Meteorol Soc 143(706):2129–2142

Martin JE (2006) Mid-latitude atmospheric dynamics: a first course. Wiley, Hoboken

Masato G, Hoskins BJ, Woollings TJ (2012) Wave-breaking characteristics of midlatitude blocking. Q J R Meteorol Soc 138(666):1285–1296

Matsueda M (2009) Blocking predictability in operational medium-range ensemble forecasts. SOLA 5:113–116

McIntyre ME, Palmer TN (1983) Breaking planetary waves in the stratosphere. Nature 305(5935):593–600

Methven J (2015) Potential vorticity in warm conveyor belt outflow. Q J R Meteorol Soc 141(689):1065–1071

Michel C, Rivière G (2011) The link between Rossby Wave breakings and weather regime transitions. J Atmos Sci 68(8):1730–1748

Mullen S (1987) Transient eddy forcing of blocking flows. J Atmos Sci 44(1):3–22

Nakamura N, Huang CS (2018) Atmospheric blocking as a traffic jam in the jet stream. Science (80-.) 361(6397):42–47

Nakamura H, Wallace JM (1993) Synoptic behavior of baroclinic eddies during the blocking onset. Mon Weather Rev 121(7):1892–1903

Nakamura H, Nakamura M, Anderson JL (1997) The role of high- and low-frequency dynamics in blocking formation. Mon Weather Rev 125(9):2074–2093

Oruba L, Lapeyre G, Rivière G (2013) On the poleward motion of midlatitude syclones in a baroclinic meandering Jet. J Atmos Sci 70(8):2629–2649

Parker TJ, Berry GJ, Reeder MJ (2013) The influence of tropical cyclones on heat waves in Southeastern Australia. Geophys Res Lett 40(23):6264–6270

Pelly JL, Hoskins BJ (2003a) A new perspective on blocking. J Atmos Sci 60(5):743–755

Pelly JL, Hoskins BJ (2003b) How well does the ECMWF Ensemble Prediction System predict blocking? Q J R Meteorol Soc 129(590):1683–1702

Pfahl S, Madonna E, Boettcher M, Joos H, Wernli H (2014) Warm conveyor belts in the ERA-Interim data set (1979–2010). Part II: moisture origin and relevance for precipitation. J Clim 27(1):27–40

Pfahl S, Schwierz C, Croci-Maspoli M, Grams CM, Wernli H (2015) Importance of latent heat release in ascending air streams for atmospheric blocking. Nat Geosci 8:610–614

Pfahl S, Wernli H (2012) Quantifying the relevance of atmospheric blocking for co-located temperature extremes in the Northern Hemisphere on (sub-)daily time scales. Geophys Res Lett 39(12):L12807

Pomroy HR, Thorpe AJ (2000) The evolution and dynamical role of reduced upper-tropospheric potential vorticity in intensive observing period one of FASTEX. Mon Weather Rev 128(6):1817–1834

Quinting JF, Jones SC (2016) On the impact of tropical cyclones on Rossby Wave packets: a climatological perspective. Mon Weather Rev 144(5):2021–2048

Quinting JF, Reeder MJ (2017) Southeastern Australian heat waves from a trajectory viewpoint. Mon Weather Rev 145(10):4109–4125

Raveh-Rubin S, Flaounas E (2017) A dynamical link between deep Atlantic extratropical cyclones and intense Mediterranean cyclones. Atmos Sci Lett 18(5):215–221

Renwick JA (2005) Persistent positive anomalies in the Southern Hemisphere circulation. Mon Weather Rev 133(4):977–988

Rex DF (1950) Blocking action in the middle troposphere and its effect upon regional climate. Tellus 2(3):196–211

Riboldi J, Röthlisberger M, Grams CM (2018) Rossby wave initiation by recurving tropical cyclones in the western North Pacific. Mon Weather Rev 146(5):1283–1301

Riemer M, Jones SC (2010) The downstream impact of tropical cyclones on a developing baroclinic wave in idealized scenarios of extratropical transition. Q J R Meteorol Soc 136(648):617–637

Riemer M, Jones SC, Davis CA (2008) The impact of extratropical transition on the downstream flow: an idealized modelling study with a straight jet. Q J R Meteorol Soc 134(630):69–91

Risbey JS, O'Kane TJ, Monselesan DP, Franzke CLE, Horenko I (2018) On the dynamics of austral heat waves. J Geophys Res Atmos 123(1):38–57

Rodwell MJ, Magnusson L, Bauer P, Bechtold P, Bonavita M, Cardinali C, Diamantakis M, Earnshaw P, Garcia-Mendez A, Isaksen L, Källén E, Klocke D, Lopez P, McNally T, Persson A, Prates F, Wedi N (2013) Characteristics of occasional poor medium-range weather forecasts for Europe. Bull Am Meteorol Soc 94(9):1393–1405

Röthlisberger M, Martius O, Wernli H (2018) Northern Hemisphere Rossby wave initiation events on the extratropical jet—a climatological analysis. J Clim 31(2):743–760

Scherrer SC, Croci-Maspoli M, Schwierz C, Appenzeller C (2006) Two-dimensional indices of atmospheric blocking and their statistical relationship with winter climate patterns in the Euro-Atlantic region. Int J Climatol 26(2):233–249

Schneider T, O'Gorman PA, Levine XJ (2010) Water vapor and the dynamics of climate changes. Rev Geophys 48(1):RG3001

Schwierz CB (2001) Interactions of Greenland-scale orography and extra-tropical synoptic-scale flow. PhD thesis, ETH Zurich

Schwierz C, Croci-Maspoli M, Davies HC (2004) Perspicacious indicators of atmospheric blocking. Geophys Res Lett 31(6):L06125

Shutts GJ (1983) The propagation of eddies in diffluent jetstreams: eddy vorticity forcing of blocking flow fields. Q J R Meteorol Soc 109(462):737–761

Sillmann J, Croci-Maspoli M, Kallache M, Katz RW (2011) Extreme cold winter temperatures in Europe under the influence of North Atlantic atmospheric blocking. J Clim 24(22):5899–5913

Small D, Atallah E, Gyakum JR (2013) An objectively determined blocking index and its Northern Hemisphere climatology. J Clim 27(8):2948–2970

Sprenger M, Wernli H (2015) The LAGRANTO Lagrangian analysis tool—version 2.0. Geosci Model Dev 8(8):2569–2586

Sprenger M, Fragkoulidis G, Binder H, Croci-Maspoli M, Graf P, Grams CM, Knippertz P, Madonna E, Schemm S, Škerlak B, Wernli H (2017) Global climatologies of Eulerian and Lagrangian flow features based on ERA-Interim. Bull Am Meteorol Soc 98(8):1739–1748

Stensrud DJ (2013) Upscale effects of deep convection during the North American monsoon. J Atmos Sci 70(9):2681–2695

Sumner EJ (1955) A study of blocking in the Atlantic-European sector of the Northern Hemisphere. Q J R Meteorol Soc 80(345):402–416

Tamarin T, Kaspi Y (2016) The poleward motion of extratropical cyclones from a potential vorticity tendency analysis. J Atmos Sci 73(4):1687–1707

Teubler F, Riemer M (2016) Dynamics of Rossby wave packets in a quantitative potential vorticity-potential temperature framework. J Atmos Sci 73(3):1063–1081

Tibaldi S, Molteni F (1990) On the operational predictability of blocking. Tellus A 42(3):343–365

Tilly DE, Lupo AR, Melick CJ, Market PS (2008) Calculated height tendencies in two Southern Hemisphere blocking and cyclone events: the contribution of diabatic heating to block intensification. Mon Weather Rev 136(9):3568–3578

Trenberth KE (1978) On the interpretation of the diagnostic quasi-geostrophic omega equation. Mon Weather Rev 106(1):131–137

Trenberth KE (1985) Persistence of daily geopotential heights over the Southern Hemisphere. Mon Weather Rev 113(1):38–53

Trenberth KF, Mo KC (1985) Blocking in the Southern Hemisphere. Mon Weather Rev 113(1):3–21

Tung KK, Lindzen RS (1979) A theory of stationary long waves. Part I: a simple theory of blocking. Mon Weather Rev 107(6):714–734

Tyrlis E, Hoskins BJ (2008a) Aspects of a Northern Hemisphere atmospheric blocking climatology. J Atmos Sci 65(5):1638–1652

Tyrlis E, Hoskins BJ (2008b) The morphology of Northern Hemisphere blocking. J Atmos Sci 65(5):1653–1665

Wernli H (1997) A Lagrangian-based analysis of extratropical cyclones. II: a detailed case-study. Q J R Meteorol Soc 123(542):1677–1706

Wernli H, Davies HC (1997) A Lagrangian-based analysis of extratropical cyclones. I: the method and some applications. Q J R Meteorol Soc 123(538):467–489

Wernli H, Schwierz C (2006) Surface cyclones in the ERA-40 dataset (1958–2001). Part I: novel identification method and global climatology. J Atmos Sci 63(10):2486–2507

Wiedenmann JM, Lupo AR, Mokhov II, Tikhonova EA (2002) The climatology of blocking anticyclones for the Northern and Southern Hemispheres: block intensity as a diagnostic. J Clim 15(23):3459–3473

Wirth V, Riemer M, Chang EKM, Martius O (2018) Rossby wave packets on the midlatitude waveguide—a review. Mon Weather Rev 146(7):1965–2001

Woollings T, Barriopedro D, Methven J, Son S-W, Martius O, Harvey B, Sillmann J, Lupo AR, Seneviratne S (2018) Blocking and its response to climate change. Curr Clim Change Rep 4(3):287–300

Yamazaki A, Itoh H (2012a) Vortex–vortex interactions for the maintenance of blocking. Part I: the selective absorption mechanism and a case study. J Atmos Sci 70(3):725–742

Yamazaki A, Itoh H (2012b) Vortex–vortex interactions for the maintenance of blocking. Part II: numerical experiments. J Atmos Sci 70(3):743–766

Zappa G, Masato G, Shaffrey L, Woollings T, Hodges K (2014) Linking Northern Hemisphere blocking and storm track biases in the CMIP5 climate models. Geophys Res Lett 41(1):135–139

Zhang G, Wang Z (2018) North Atlantic extratropical Rossby wave breaking during the warm season: wave life cycle and role of diabatic heating. Mon Weather Rev 146(3):695–712